

LV-2015-039



Landsvirkjun



# Tectonic Control of Alteration, Gases, Resistivity, Magnetics and Gravity in Þeistareykir Area

Implications for Northern Rift Zone and Tjörnes Fracture Zone



Report no: LV-2015-039



# Tectonic Control of Alteration, Gases, Resistivity, Magnetics and Gravity in Þeistareykir Area

Implications for Northern Rift Zone  
and Tjörnes Fracture Zone



ÍSOR-2015/002

Project no.: 14-0207

March 2015



## Key Page

LV report no: LV-2015-039 Date: March 2015Number of pages: 59 Copies: 11 Distribution:  On [www.lv.is](http://www.lv.is)  
 Open  
 Limited until

Title: Tectonic Control of Alteration, Gases, Resistivity, Magnetics and Gravity in Peistareykir Area. Implications for Northern Rift Zone and Tjörnes Fracture Zone.

Authors/Company: Maryam Khodayar, Sveinbjörn Björnsson, Ragna Karlsdóttir, Kristján Ágústsson and Magnús Ólafsson

Project manager: Ásgrímur Guðmundsson (LV) Magnús Ólafsson (ÍSOR)

Prepared for: Prepared by Iceland GeoSurvey (ÍSOR) for Landsvirkjun.

Co operators:

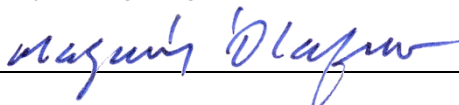
**Abstract:** We present results of Phase 2 of the structural analysis of Peistareykir in the Northern Rift Zone and the Tjörnes Fracture Zone: (a) The statistical analysis of the fractures deduced from aerial images in the 2400 years lava, postglacial, and Quaternary/Upper Tertiary series indicates that the WNW, NNE, ENE, NW/NNW and E-W Riedel shears of the transform zone dominate in the 2400 years lava. As rocks become older, the northerly fractures turn to be more frequent, up to 10% of the total fracture population. (b) The tectonic control of the alteration, gases, resistivity structures, aeromagnetic and gravity reflect the same mechanisms. The Riedel shears control dominantly the location and distribution of the alteration and gases in Peistareykir. The resistivity structures display striking en échelon arrangements indicative of dextral and sinistral deformation controlled by WNW to NW, NNE, ENE and NW Riedel shears, and secondarily by small northerly lineaments. The Riedel shears also appear in the magnetic and gravity structures. (c) At crustal depth, the tectonic lineaments controlling the resistivity structures undergo a gradual clockwise rotation, up to 40°E, from 1000 to 4000 m b.s.l., an anti-clock rotation of 4° to 16° W at 5000 and 6000 m b.s.l., and again a clockwise rotation of 2° to 14° E at 8000 m b.s.l. The Riedel shears dominate the upper 6000 km in the crust, but at 8000 b.s.l., few N-S, E-W, WNW and NNW lineaments equally control the tectonic configuration. The E-W is the deepest set of fracture appearing from 4000 m b.s.l., which explains why E-W fractures are so uncommon at the surface. (d) All lineaments identified from sub-surface coincide with the fractures mapped from the surface. (e) Among the Riedel shears, the WNW dextral strike-slip fault of Stórhver-Bæjarfjall plays a significant role in the geothermal activity, in the 2400 years old eruption, and in the formation of northerly pull-apart structures within the fissure swarm. (f) Further analysis on the dip-slips, shear zones, common weak zones, and the depths of the fractures from boreholes is needed to provide a ground for drillings in Peistareykir. We recommend carrying these tasks in Phase 3 of the structural analysis of Peistareykir.

**Keywords:** Northern Rift Zone; Tjörnes Fracture Zone; Geothermal alteration and gases; Block rotation; Resistivity structures; Fractures; Pull-apart

ISBN no:

Approved by Landsvirkjun's  
project manager

Project manager's signature



Reviewed by

SGK



## Table of contents

<b>1</b>	<b>Introduction.....</b>	<b>7</b>
<b>2</b>	<b>Geological context.....</b>	<b>8</b>
<b>3</b>	<b>Surface geological data .....</b>	<b>9</b>
3.1	Correlation with other structural maps .....	9
3.2	Statistical analysis of the mapped structures per age .....	11
3.3	Surface geothermal alteration .....	13
3.3.1	Correlation with other alteration maps .....	13
3.3.2	Tectonic structures controlling surface geothermal alteration.....	14
3.4	Geochemical analysis of gases in steam.....	16
3.5	Structural interpretation of gases and alteration.....	17
3.5.1	Fracture segments in the distribution and concentration of gases .....	17
3.5.2	Fracture segments influencing the gases and alterations .....	19
3.6	Recall of the shift of Þeistareykir fissure swarm .....	19
<b>4</b>	<b>Sub-surface geophysical data .....</b>	<b>20</b>
4.1	Tectonic control of the resistivity structures .....	21
4.1.1	A note on the width of the resistivity structures.....	21
4.1.2	Structural analysis of the resistivity data and correlation with fractures	22
4.1.3	Rotation in the tectonic structures and depths of the fractures .....	24
4.2	Brief correlation with magnetic and gravity maps.....	27
<b>5</b>	<b>Summary and Recommendations .....</b>	<b>28</b>
<b>6</b>	<b>References.....</b>	<b>30</b>

## List of tables

Table 1. <i>Summary of the fracture sets, their frequencies at each depth, the amount and sense of rotation.</i> .....	26
--	----

## List of figures

Figure 1. <i>Overview of geological context.</i> .....	34
Figure 2. <i>Recall of some results from Phase 1 of structural analysis of Þeistareykir</i> .....	35
Figure 3. <i>Correlation of our tectonic lineament map with previous structural maps also made from images.</i> .....	36
Figure 4. <i>Statistical analysis per relative age of the fractures interpreted from aerial image</i> ...	37

Figure 5. <i>The mapped alteration in Tjarnarás, Bæjarfjall, Ketilfjall and Þeistareykir in the field and from aerial images</i> .....	38
Figure 6. <i>Location and tectonic control of alteration in Þeistareykir and immediate surroundings</i> .....	39
Figure 7. <i>Concentration, distribution, ratio of geochemical elements in steam, and gas provinces at Þeistareykir</i> .....	40
Figure 8. <i>Our tectonic interpretation of the concentration, distribution, and ratio of geochemical elements in steam at Þeistareykir</i> .....	41
Figure 9. <i>Our tectonic interpretation of the concentration of geochemical elements in steam as well as the gas temperatures at Þeistareykir</i> .....	42
Figure 10. <i>Correlation between lineaments emerging from tectonic interpretation of gases, alteration, and interpreted weak zones</i> .....	43
Figure 11. <i>New explanation as to the mechanism responsible for the shift of the structures in the Þeistareykir fissure swarm</i> .....	44
Figure 12. <i>Frame of TEM/MT survey compared to the fracture map, and type of results showing the resistivity structures</i> .....	45
Figure 13. <i>Structural interpretation of the resistivity structures at 0 m</i> .....	46
Figure 14. <i>Structural interpretation of the resistivity structures at 500 m b.s.l.</i> .....	47
Figure 15. <i>Structural interpretation of the resistivity structures at 1000 m b.s.l.</i> .....	48
Figure 16. <i>Structural interpretation of the resistivity structures at 1500 m b.s.l.</i> .....	49
Figure 17. <i>Structural interpretation of the resistivity structures at 2000 m b.s.l.</i> .....	50
Figure 18. <i>Structural interpretation of the resistivity structures at 2500 m b.s.l.</i> .....	51
Figure 19. <i>Structural interpretation of the resistivity structures at 3000 m b.s.l.</i> .....	52
Figure 20. <i>Structural interpretation of the resistivity structures at 4000 m b.s.l.</i> .....	53
Figure 21. <i>Structural interpretation of the resistivity structures at 5000 m b.s.l.</i> .....	54
Figure 22. <i>Structural interpretation of the resistivity structures at 6000 m b.s.l.</i> .....	55
Figure 23. <i>Structural interpretation of the resistivity structures at 8000 m b.s.l.</i> .....	56
Figure 24. <i>Structural interpretation of aeromagnetic data</i> .....	57
Figure 25. <i>Structural interpretation of the Bouguer gravity map</i> .....	58
Figure 26. <i>Structural interpretation of the Residual anomalies</i> .....	59



# 1 Introduction

The Þeistareykir geothermal field is in the westernmost fissure swarm of the Northern Rift Zone, but also within the Tjörnes Fracture Zone (Figs. 1a to 1c). Due to this configuration, the geothermal field is subject to the tectonic of the rift and transform plate boundaries. The exploration of Þeistareykir geothermal field has included geological mapping, resistivity, surface alteration, water geochemistry, and gas geothermometry (Sæmundsson, 2007; Gíslason et al., 1984; Karlsdóttir et al., 2012; Kristinsson et al., 2013a; Óskarsson, 2011). Although the relevant contribution of Gíslason et al. (1984) laid the ground for the better understanding of such tectonic, an updated structural analysis that depicts in more detail the effects of both types of plate boundaries is not at hand. Most recent geological maps, in fact, show a fracture pattern mostly dominated by the northerly extensional faults and fractures of the rift (Fig. 1c).

As geothermal fields are fracture controlled in Iceland, it is critical to have a thorough structural analysis and the models based on a variety of available data. Interpretation of such multidisciplinary data results in detecting the tectonic configuration, but also the most important structures that play a role in the exploration and exploitation of the resources. To this end, we proposed to Landsvirkjun a multidisciplinary tectonic analysis in several steps. During the first phase of the project, we re-interpreted the fracture pattern of Þeistareykir and surroundings from 8 types of aerial images (Khodayar and Björnsson, 2013). Using these observations, we prepared a new structural map where six sets of fractures, most with normal and some with strike-slips displacements, are spread throughout the region (Map 1). As the observations are from the surface, the depths of the fractures into the crust are unknown, so are their roles in the control of geothermal activity and how they correlate with other known structures from sub-surface data.

The present work is Phase 2 of the project. In this work we use results of Phase 1 in a tectonic analysis and interpretation of both surface geological and sub-surface geophysical data to provide a more in-depth picture of the role of tectonic. The objectives of the present work are the following.

From surface:

- Correlation of the structural map of Phase 1 with similar existing fracture maps.
- Statistical analysis of the fracture sets of Phase 1 based on their age.
- Interpretation of the tectonic control of surface alteration, and correlation with previous alteration maps.
- Highlight of major structures as stemming from our analysis and interpretation.

Although not a part of the initial plan, we found it necessary to undertake an additional task, which is the analysis and correlation of the geochemical data from Gíslason et al. (1984) as the data is highly relevant for the tectonic control of alteration.

From sub-surface:

- Structural interpretation of the latest resistivity data (Karlsdóttir et al., 2012).

Although new gravity and aeromagnetic maps are not at hand yet, it became apparent during our multidisciplinary analysis that a brief correlation with existing gravity and aeromagnetic maps (Gíslason et al., 1984) is relevant to our tectonic interpretation. Therefore, we undertook the additional task of this multidisciplinary correlation.

It is emphasized that results of each Phase of the project provide one step forward in understanding the tectonic control relevant to geothermal activity. It is anticipated that results of this phase need to be correlated with borehole data in an ulterior effort, or during Phase 3, in order to provide the most comprehensive overview of the role of the structures.

## 2 Geological context

The Þeistareykir geothermal field is a part of the Þeistareykir/Mánáreyjar fissure swarm of the Northern Rift Zone (NRZ). The field and its surroundings in this rift segment are also located within the transform zone of Tjörnes Fracture Zone (TFZ), more precisely, between the Húsavík-Flatey Fault and the Dalvík lineament (Fig. 1a). The geothermal field and its surroundings undergo deformation from these two types of plate boundaries. The tectonic history of this part of Northern Iceland is complex and includes plate reorganisations, flexuring, intense fracturing, and rotation over several million years (e.g., Sæmundsson, 1978; Voight and Mamula, 1983; Jancin et al., 1985; Young et al., 1985; Garcia et al., 2002).

The series found in Þeistareykir-Mánáreyjar swarm consist of lavas and hyaloclastites, with local rhyolite at Mælifell to the northwest of Þeistareykir, as well as andesite and dacite. The bed rock spans Miocene to interglacial and subglacial series (Bruhnes-Weischselian), including volcanic material and the Pliocene marine fossil-rich Tjörnes bed. The postglacial lavas are younger than 15000 years, and the last eruption of 2400 years ago emitted the picrite Þeistareykir lava from the Stórhver crater (Sæmundsson et al., 2012a). But contrary to the Krafla fissure swarm, no apparent volcanic centre stands out in Þeistareykir and acidic rocks are insignificant at the surface.

The TFZ is some 120 km long and about 70 km wide. However, the transform zone is believed to have been active at least 6–7 Ma, and has both subsidence in order of hundreds of metres and a dextral shift of some 100 km (e.g., Sæmundsson, 1978). Presently, the TFZ consists of three major WNW trending structures, the Grímsey Oblique Rift, the Húsavík-Flatey Fault (HFF) and the Dalvík Lineament. The HFF presents an established fault plane in the outcrop, showing dextral motion as confirmed by offshore earthquakes on the fault plane itself (Rögnvaldsson et al., 1998). The Dalvík lineament has a sharp signature in the topography in its eastern part, but earthquakes are recorded mostly in the western part of this structure on north-easterly sinistral strike-slips to the north of the lineament (Stefánsson et al., 2008). GPS measurements (Geirsson et al., 2010) indicate continuous deformation of the TFZ, with earthquakes up to M7 (Einarsson and Björnsson, 1979). One or two earthquakes >M6 have occurred on each of

the three transform lineaments in the last three centuries. Focal mechanisms of earthquakes in the TFZ indicate strike-slip motions on northerly, NNE/NE, WNW and NW fracture segments (Rögnvaldsson et al., 1998), supported by relocated earthquakes at Þeistareykir (Hjaltadóttir and Vogfjörð, 2011). A number of investigations both in the adjacent old crust of Flateyjarskagi (Voight and Mamula, 1983; Young et al., 1985; Mamula and Voight, 1985), and in the younger series of Þeistareykir (Gíslason et al., 1984) also show existence of these sets of fractures, which are typical of transform faulting. On geological maps (Fig. 1c), however, the fracture pattern of Þeistareykir and surroundings are favourably northerly normal faults and open fissures parallel to the rift, and a few WNW segments (e.g., Sæmundsson et al., 2012b).

Results of our preliminary structural analysis from aerial images are complementary to the existing tectonic knowledge of the area. The presence of several sets of fractures at Þeistareykir and surrounding, similar to those during earthquakes associated with TFZ, are easily recognisable on aerial images (Map 1 and Fig. 2a) (Khodayar and Björnsson, 2013). Based on the frequency and distribution of these fractures, we suggested the existence of tightly parallel weak zones throughout the region (Fig. 2b). On the ground of their surface geometry and motions, we grouped the fractures into purely extensional normal faults and open fractures parallel to the rift (northerly), and 4 sets of oblique-slip structures having dextral (WNW, NW/NNW) and sinistral (NNE and ENE) motions. The sixth set of fracture, striking E-W, is the most discreet. It has the shortest traces and presents no apparent evidence of strike-slip (Fig. 2c). Overall, the faults in the older rocks have sharper traces and higher magnitude of vertical displacement, but finer and more subtle traces along with least dip-slip in the younger lavas. This is indicative of long activity and slip-accumulation.

All sets of fractures identified from aerial images but the northerly set act as Riedel shears related to transform faulting (Khodayar and Björnsson, 2013), with strikes and motions here that are compatible with the spreading direction of N105°E identified by DeMets et al. (2010) (Fig. 2c). In total, we mapped 10729 fracture segments of variable lengths from aerial images. Their statistical analysis showed that the northerly fractures are the most frequent, but they constitute less than 10% of the total fracture population (Fig. 2d). Not only the frequency of non-rift-parallel fractures is high at Þeistareykir and surrounding, some of the Riedel shears have critical roles in the geological processes. As example, we suggested that the last eruption in the central part of Þeistareykir fissure swarm (2400 years ago) occurred on a WNW dextral fracture segment stretching from Stórhver to Bæjarfjall (Figs. 2a and 2b).

## **3 Surface geological data**

### **3.1 Correlation with other structural maps**

Two main works similar to ours that were prepared from aerial images are available for correlation.

In an excellent work, Gíslason et al. (1984) prepared a tectonic lineament map mostly from aerial photographs. On the map, the fractures are differentiated based on their age,

i.e., younger fractures (formed or reactivated during postglacial time (8000–15000 years), and older (> 15000 years, including Quaternary and Upper Tertiary), as well as their types (normal faults, open fractures, and a few strike-slips). The tectonic lineament map shows that in addition to northerly extensional fractures of the rift, three other sets exist at Þeistareykir and regionally (Fig. 3a). These sets strike WNW, NE, and to a lesser degree E-W. All sets display apparent normal-slip dipping as much towards one direction than the other. Strike-slip is mentioned mostly along the Húsavík-Flatey Fault (HFF), and another fault with similar strike. All fracture sets appear in rocks older than Holocene where their apparent throws are reported as  $\geq 200$  m. But in the southern part of the 2400 years old Þeistareykir lava, only northerly and WNW-NW faults are identified and labelled as young fractures and normal-slip.

A more recent tectonic lineament map by Magnúsdóttir and Brandsóttir (2011) is made from aerial photographs and satellite images (Spot5) onland, and bathymetric images from multibeam data (2002) offshore. On this map (Fig. 3b) the lineaments are predominantly northerly, stretching from southwest of Bæjarfjall northward to the east of Mánáreyjar offshore. In the middle of Þeistareykir fissure swarm onland, the HFF is mapped as series of WNW lineaments with dextral motion, along with shorter WNW lineaments just north of the HFF with sinistral motion. A few ENE lineaments are also identified at Kelduhverfi and offshore to the east and northeast of Mánáreyjar. Northerly rift-parallel fractures are rightly interpreted as forming horsts and grabens. However, they are classified into two distinct parallel domains: (a) Normal faults, all interpreted as eastward dipping, occupy the older rocks of the highland to the west of the Þeistareykir swarm; (b) Rift fissures to the east of the normal faults, mostly in the younger lavas of the lowland. The statistical analysis by the authors suggests the mean azimuths of the northerly fractures as  $N21^{\circ}E$  to  $N27^{\circ}E$ , and that of Kelduhverfi as  $N43^{\circ}E$ . The variety in the strikes and motions of the fracture sets are mostly attributed to local fluctuation of extension across the fissure swarm, i.e.,  $N107^{\circ}E$  to the north and east of HFF and  $N90^{\circ}E$  south of it. Further work on the tectonic of Þeistareykir by Magnúsdóttir and Brandsóttir is in preparation, but results are not published yet for correlation.

Our fracture map (Khodayar and Björnsson, 2013) benefited from several advantages (Fig. 3c). Firstly, we used a greater variety of aerial images onland, namely pairs of aerial photographs in monochrome, orthomaps from two different years and in two different colors, as well as spot5 images in three different channels. Due to their scales and resolutions, the images provided complementary depths to the observations for better identifying the fractures. Our interpretation results from the analysis of these 8 types of images combined. Secondly, we transferred to Þeistareykir not only our knowledge of similar structural analysis from aerial images analysis but also from field work in the rift and transform segments of West, South, and Southwest Iceland. These advantages resulted in a more exhaustive picture of the fracture sets, their distribution (Fig. 3c), motions and stress condition (Fig. 3d).

Practically, the similarities and differences between the three fracture maps are as follows:

(a) The map of Magnúsdóttir and Brandsóttir emphasises the northerly set of the rift where the fracture traces are identical to those of Gíslason et al. (1984).

(b) As on the map of Gíslason et al., we see the normal faults and open fissures spread throughout the area and not occurring in two distinct domains as appears on the map of Magnúsdóttir and Brandsdóttir (2011). It is obvious that younger postglacial fractures in the central part of Þeistareykir swarm have normal-slips, even if their throws are less than the faults in the older lavas. Furthermore, the young fractures do not appear only within the postglacial lavas. They appear also in older rocks though to a lesser degree.

(c) Similar to Gíslason et al. (1984), we observe that northerly normal faults are not all dipping eastward in the western part of the Þeistareykir fissure swarm, but they dip both to the east and west there, even if locally a group of faults may dip in a favoured direction.

(e) Overall, our interpretation is more similar to that of Gíslason et al. (1984). Except that we provide a more exhaustive picture of the tectonic at local and regional scales due to the following contributions. We: (a) Identified a higher number of fracture sets (six in total); (b) Classified the lineaments in terms of age, traces (major, minor, faint); geometries (open, normal faults, undifferentiated); (c) Recognised strike-slip motions (dextral and sinistral) along more fracture sets and a higher number of individual fractures; (d) Identified the normal-slip and dip-direction along most of the faults; (e) Provided kinematic and dynamic interpretation explaining the six fracture sets under a single stress field that is compatible with regional stress and the two types of plate boundaries.

In the following chapters, the correlations of our tectonic lineament map with other types of data will shed lights on the existence of a complex fracture pattern as suggested in our study.

## 3.2 Statistical analysis of the mapped structures per age

Our preliminary statistical analysis (Khodayar and Björnsson, 2013) used the totality of the mapped fractures at once without any distinction (Fig. 2d). Surely the northerly rift-parallel fractures constitute an obvious part of the tectonic pattern, but due to the presence of even a higher number of oblique-slip Riedel shears of the transform zone, it is beneficial to know more about the mechanism of formation of these fractures. Within the limited frame of this work, we address the issue by dividing the fractures into three main age groups based on the age of the host rock (Fig. 4). Before presenting the results of our analysis, three aspects should be mentioned:

- Although this approach is very simplistic, because new fractures can form in older rocks but they will be counted as old, the method itself allows obtaining some hints as to the overall mechanism of fracture formation. A more thorough statistical analysis is needed in the future steps of our work to find ways of correcting the above aspects and some other potential uncertainties. Therefore, we emphasise that, even if there are uncertainties in grouping the fractures according to the age of the rock here, the younger fractures in the old rock would not change the overall results in any significant way due to the high number of fractures used in the statistical analysis.

- We also emphasise that despite the number of fracture is high on our maps (i.e. Map 1), not all of the fractures have the same weight. Some are major and obvious in the field due to their substantial vertical displacement and their role in shaping the landscape. Others, however are secondary (shorter with less throw), and even faint (hair-like, undetectable in the field but visible on aerial images for trained eyes).
- When the number of fractures involved is very high and the area covered large (for example several hundred fractures over many kilometres), we use the length of the fractures for calculation of the strikes rather than the number of segments. This approach is based on our experience that, although fractures with shorter length have significant role in reflecting the deformation and adjusting the blocks kinematically, they do not have the same weight as longer fractures and thus may blur the picture as to the frequency of the strikes. This is explained in more detail in a recent short report by Khodayar and Víkingsson (2015).

For the more detailed statistical analysis of the fracture population, we grouped the fractures into three groups of wide age-interval (Figs. 4a and 4b). One group (group 1) consists of obviously the youngest fractures as these are found in the 2400 years old Peistareykir lava (Fig. 4c). The second group (group 2) consists of fractures cutting through the postglacial lavas, which range between 8000 and 15000 years in age (Fig. 4d). The postglacial lavas surround the Peistareykir lava. And the last group (group 3) comprises all fractures mapped in the oldest lavas and hyaloclastites, i.e., more than 15000 years, which cover both the Quaternary and the Upper Tertiary (Fig. 4e).

The rose diagram representing the fracture sets in each of the three groups reflects the role of the two types of plate boundary in time:

- In group (1) in the 2400 years old Peistareykir lavas, the ENE fracture sets dominate, followed by WNW and NNE sets (Fig. 4c). The northerly, NW and E-W sets are the least frequent here. Fractures in these lavas are minor or have even faint traces, which stems from the fact that they are young and have not yet reached a full development. The features of these Riedel shears are obvious indications that at least in this part of Northern Iceland, young fractures form dominantly under the influence of the transform zone.
- Rifting is more developed in group (2) in the postglacial lavas (8000–15000 years old), as fractures in the interval of  $N0^{\circ}$ – $20^{\circ}E$  are the most frequent if individual strikes are taken into account (Fig. 4d). Secondarily, the ENE ( $N50^{\circ}E$ – $N70^{\circ}E$ ), and WNW ( $N110^{\circ}E$ – $130^{\circ}E$ ) seem dominant. Fractures with the strike-interval corresponding to Riedel shears are by far the most frequent.
- In the lava pile > 15000 years old of group (3) that span Quaternary and Upper Tertiary, the same frequencies appear as in group (2), but additionally, fracture striking NW/NNW ( $N150^{\circ}E$ – $N160^{\circ}E$ ) are more prominent with age (Fig. 4e).

In short, the above statistical analysis shows that fracture form under the influence of the transform zone here, and only with time the effect of rifting becomes apparent in the tectonic pattern. Both the transform zone and the rift have critical roles in the development of fractures with time.

### 3.3 Surface geothermal alteration

Three main works on the status of surface alteration, gas concentration and the tectonic control of geothermal activity are available for correlation with our findings below.

#### 3.3.1 Correlation with other alteration maps

The alteration map of Gíslason et al. (1984) is the earliest comprehensive map giving a detailed view of the geometry and distribution of surface geothermal alteration (Fig. 5a). The alteration is distinguished as soil and deposition, steam and snow melt, as well as mud pots and springs. The alteration is clearly concentrated to the north and west of Bæjarfjall where the largest coverage is a continuous altered zone at Tjarnarás Fault and south of it. The last outcrops where patches of small alteration and snow melt were mapped are at maximum 1 km to the west and northwest of Bæjarfjall.

The map of Ármannsson et al. (2000) shows the status of alteration between 1983 and 1991 around Bæjarfjall (Fig. 5b). The map does not distinguish between the type of surface alteration and geothermal activity, but provides an overall contour of the alteration zone in the same areas as mapped by Gíslason et al. (1984). Based on surface temperature in the alteration zone, Ármannsson et al (2000) suggest that the area to the west of Tjarnarás Fault (or northwest of Bæjarfjall) is colder in 1991 than it was in 1983–1984. Small patches at Ketilfjall and to the southwest are shown as being partly cold and partly hot in 1991, but the main hot area is in the middle part of the alteration zone to the north of Bæjarfjall (Fig. 5b).

Recent monitoring of surface manifestations by Kristinsson et al. (2013a; 2013b) in the field shows the status of geothermal activity during the years 2012 and 2013 with no major change (Fig. 5c). Gas measurements indicate that the hottest area in 2012 is a small vent at Ketilfjall. The area in the middle part of the alteration zone to the north of Bæjarfjall that was the hottest in 1991 appears still to be hot in 2012 (Fig. 5c). Mapping of geothermal surface manifestations by Kristinsson et al. (2013a) confirms that the most active area is in the middle of the overall alteration zone to the north of Bæjarfjall. The authors also show that the activity has somewhat declined to the southwest of Ketilfjall, but has increased to the southwest of Bæjarfjall. The area at Tjarnarás Fault is the least active in 2012 as in 1991.

The above efforts demonstrate that the surface geothermal activity, alteration and temperatures change rapidly in the space of a decade or two.

We mapped the alteration based on their contrast with the surrounding bedrock on aerial images (Fig. 5d). However, our observations are influenced by our field mapping experience of identical altered zones in other low and high-temperature geothermal fields in Iceland. We observed three categories of surface alterations on the images: (a) White strong, with the most prominent signature, corresponding to highly altered soil; (b) White possible, which has more faint signature but presents enough contrast to be differentiated from bedrock; (c) Dark possible, which based on field experience, could correspond to clay in a very mild geothermal alteration. The strong white alteration is concentrated to the north, northwest and west of Bæjarfjall, as well as a single small patch to the north of Stórhver near Skildingaholt, i.e., at ~1 km to the northwest of

Tjarnarás Fault (Fig. 5d). This category matches well the main alteration zones mapped by previous co-workers. The white possible alteration is observed in two areas, one to the northeast of Bæjarfjall (at Ketilfjall and Bóndhóll), and the other to the southwest of Bæjarfjall at ~ 1.5 km south of the strongest alteration. The dark possible alteration is observed in very narrow zones localised to the north of Ketilfjall and around the small patch to the north of Stórhver.

Our mapping of the alteration from aerial images and the mapping of Gíslason et al., (1984) and Kristinsson et al. (2013a) in the field match satisfactorily, even if in detail there are variations in the geometry of the mapped alterations. What all of these mappings have in common is that neither from aerial images nor from the field, does surface geothermal alteration appear beyond the area around Bæjarfjall. Below, we interpret the structural control of the geothermal activity that explains the location and distribution of the surface manifestations.

### **3.3.2 Tectonic structures controlling surface geothermal alteration**

On the map of Gíslason et al. (1984) and Kristinsson et al. (2013a), the altered soils are predominantly elongated N-S to the west of Bæjarfjall, except at Tjarnarás where a part of the altered soil change orientation from N-S to NNW, as well as farther west where a smaller patch has a NE orientation (Fig. 5a). At the opposite side to the east, surface alteration is organised northerly, stretching from Ketilfjall towards Bæjarfjall on both maps. In the middle altered zone to the north of Bæjarfjall, the hottest soils are organised NW, WNW, N-S and ENE (Fig. 5a and 5c). In this zone, Kristinsson et al. (2013a) show the surface geothermal manifestations as aligned on short N-S parallel zones within an overall E-W zone, but Gíslason et al. (1984) show the alteration as one main N-S zone to the east and one WNW zone just to the west of the N-S zone. The two maps also display a series of faults and open fractures with, however, slight differences. On both maps, N-S faults and open fractures are shown coinciding with the N-S hottest altered soils in the middle part of Bæjarfjall to the north. Sæmundsson (2007) mapped a few more northerly faults to the west of Bæjarfjall, extending under the northerly alteration to the south of Tjarnarás (Fig. 5c). On the map of Gíslason et al. (1984), the Tjarnarás Fault is shown as a single normal fault plane bending from N-S to the north, to NW southwards and then to WNW in Bæjarfjall. A shorter WNW lies parallel to the WNW portion of this fault in Bæjarfjall. Noticeably, the fault plane presents a major bend along its trace. Kristinsson et al. (2013a; 2013b) mapped the Tjarnarás Fault as N-S to the north with a slight bend to NW to the south. The fault plane appears discontinuous before entering Bæjarfjall as a short NW segment. However, none of these two maps show fractures coinciding with the alteration zone in the middle part of Bæjarfjall to the north, and generally there are no other WNW, E-W or NE fractures on these maps except the fractures described above.

Although the shapes of surface alteration that we mapped are similar to those of Gíslason et al. (1984) and Kristinsson et al. (2013a; 2013b), our structural interpretation of the geothermal activity differs from the two previous works, partly because we have at hand a more thorough structural map and partly because we use a different approach in our interpretation.



In order to visualise the regional extent of the alteration, we outlined the boundaries beyond which the altered soils are not reported in the immediate surroundings in any of the works (Fig. 6a). These outlines are drawn respecting the elongation of the altered soils themselves, not the least along which strikes the outcrops are best connected. From this approach, it appears that the alteration is contained in a “block” with an overall strike of N15°E, but the strikes of the boundary of the “block” are locally different particularly to the west. From north to the west, the boundary of the “block” could be N117°E far north of Ketilfjall, N 46°E from north of Stórhver north-eastwards, N162°E at the latitude of Tjarnarás, N15°E and then N135°E to the west and south of Tjarnarás, and finally N15°E in south of Bæjarfjall in Borgarhraun (Fig. 6a).

We then superimposed the alteration “block” on the summary of the weakest zones among our mapped tectonic lineaments (Figs. 6b, 2a and 2b). This attempt explains both the outer boundaries of the alteration “block” and the alignments of the alteration zones within the “block”:

- (a) The structures marked as 1, 2, 3, and 4 on Figure 6b are the outer boundary of the alteration “block”. They correspond respectively to the WNW set with dextral motion, NNE to ENE with sinistral motion, NW-NNW with possible dextral motion, and northerly extensional sets. As a reminder, all sets with strike-slip motion display also normal-slip. The structures marked as 1a, 2a, 3a, etc., represent those fractures that play a role in the control of geothermal activity inside the alteration “block”.
- (b) In detail, structure (1) that could delimit the northern edge of the alteration “block” is on the trace of the HFF. Other WNW structures are 1a, on which the dark possible alteration align; (1b) from which the possible white alteration declines northwards; (1c) controlling the overall alignment of the hottest soils on the northerly part of Bæjarfjall. This structure and the segment at Stórhver could belong to the same major dextral fault, responsible of both the geothermal activity and the biggest postglacial eruption within the Þeistareykir swarm.
- (c) The structure 2 bounds the alteration “block” to the northwest along two en échelon NNE fault segments with sinistral motion and dip-directions to the northwest (Fig. 6b). Other structures with sinistral motion are a series of parallel ENE faults inside the block where (2a) controls the ENE elongation of the dark possible alteration; (2b) where three parallel segments control the geothermal activity within the central part of the alteration “block”. We interpreted the micro-earthquakes from 1993 to 2011 (Hjaltadóttir and Vogfjörð, 2011) on the northern slope of Bæjarfjall as occurring on these ENE sinistral fault segments (Khodayar and Björnsson, 2013); (2c) is the sinistral fault segment with mostly open fractures controlling both the NNE white possible alteration to the southwest of Bæjarfjall and the strong white alteration adjacent Tjarnarás.
- (d) The structures labelled as (3) and (3a) are two narrow parallel faults, one of which is the NNW Tjarnarás Fault on which the strong white alteration occur (3a), and the other bounds the outer edge of the alteration “block” to the west. These structures extend both south-eastwards in Bæjarfjall, but also north-westwards and seem in the continuation of the NNW segments of Sæluhúsmúli-Grísatunga,

which present normal-slip (Fig. 6b). We interpreted the geometry of the open fractures at Sæluhúsmúli-Grísatunga as evidence of possible dextral motion along the fault segments there. Our suggestion is supported by micro-earthquakes, which show dextral motion on the trace of Tjarnarás Fault (Khodayar and Björnsson, 2013).

- (e) Finally, the northerly structures labelled as (4) control the overall N15° E strike of the alteration “block” and are purely extensional, belonging to the rift. The structure (4) to the east could also coincide with the eastern boundary of Þeistareykir fissure swarm since beyond this fracture to the east, no major northerly fault appears on the images in the immediate surroundings (Fig. 6b). Other northerly structures are (4a) at Ketilfjall giving rise to the northerly alignment of geothermal manifestations there, as well as the bend of the dark possible alteration to northerly farther north on the trace of this westward-dipping fault. The structure (4b) is a short segment that is responsible for the northerly strike of the Tjarnarás Fault, as well as the northerly alignment of the alteration there. The structure (4c) is an open fractures / young westward dipping normal fault that bounds the white possible alteration within the alteration “block”. Beyond this structure to the east, no convincing evidence of alteration was observed on the images.

Besides an in-depth and updated interpretation of the structures that control the geothermal activity, our analysis also brings an important hint as to the mechanism of diverging plate boundaries where rift and transform zones interact in the same location: As their strikes and motions indicate, the tectonic pattern observed here is a blend of rift-parallel northerly extensional fractures and the strike to oblique-slip Riedel shears of the transform zone. In this pattern, the proportion of the Riedel shears is higher, indicating that the geothermal activity is dominantly controlled by the transform zone and secondarily by rift.

### 3.4 Geochemical analysis of gases in steam

Monitoring of gases in Þeistareykir geothermal field has been undergoing for more than half a century (e.g., Hermannsson and Línadal, 1951; Gíslason et al., 1984; Ármannsson, 2004; Kristinsson et al., 2013a). One of the relevant works is that of Gíslason et al. (1984) where results of gas concentrations and assessment of the reservoir temperature based on geothermometer calculations uses a sufficient number of sampling locations (Figure 7a). Additionally, results of Gíslason et al. (1984) are plotted on several maps (Figs. 7b to 7k), ready for correlation with our structural data.

On Fig. 7, we reported the concentrations, ratios, and distribution of several chemicals as measured by Gíslason et al. (1984) in fumarole at Þeistareykir. Although an in-depth analysis is not at hand to determine at what depths the gases generate to reach the surface, assumptions on their relative depths indicate that (Ármannsson, 2015; pers. comm.) the deepest gases could be H<sub>2</sub> (Fig. 7b) and CO<sub>2</sub> (Fig. 7c), coming respectively from 5–7 km and 5–6 km depth. H<sub>2</sub>S (Fig. 7d) and methane (Fig. 7e) are generally shallower, possibly coming from 3–4 km and 2–3 km depths, respectively. The ratio of <sup>18</sup>O/<sup>16</sup>O in Þeistareykir has been used to determine the direction of the flow of ground

water here at a depth of 2–3 km (Fig. 7f). Chloride (Fig. 7g) and Radon (Fig. 7h) do not give a definite hint as to a depth because they can be generated from fluid that interacts with rock at any depth. Due to its low concentration in Þeistareykir, it may be assumed that Chloride does not come from a great depth either. Finally, three maps estimate the average gas temperature (Fig. 7i), CO<sub>2</sub> gas temperature (Fig. 7j), and H<sub>2</sub>S gas temperature (Fig. 7k). They indicate the hottest and cooler areas.

The relative depths and shapes of gas concentrations and their distribution are relevant for our structural analysis. But before attempting a correlation with our mapped structures and an overall structural interpretation, two points should be emphasised.

- (a) Through an ENE transect cutting the data points, Gíslason et al. (1984) and Guðmundsson et al. (2008) suggest 5 gas provinces labelled as (A) to (E) (Fig. 7l). Area (C) is the hottest and in fact corresponds to location of the hottest geothermal manifestations at the surface to the north of Bæjarfjall (Figs. 5a to 5c). Areas (C) and (D) at Þeistareykir and Tjarnarás, as well as (A) at Ketilfjall are likely steam-dominated at depth and these are the areas where steam is observed at the surface as well. While area (E) to the west of Tjarnarás as well as are (B) at Bóndhóll are with condensate at depth and thus without steam at the surface. The authors show prominent boundaries separating these provinces (Fig. 7l). The boundaries between provinces (A), (B) and (C) are WNW-NW, that between (C) and (D) is rather NW-NNW, and that between areas (D) and (E) is NNW-NS.
- (b) The suggested linear boundaries between gas provinces rightly reflect some of the underlying NW and northerly structures that control such compartmentalisation (Fig. 7l). However, the fractures shown on Fig. 7 neither explain all of the overall boundaries, not the detailed distributions and concentrations of gases. Below, we provide a new structural interpretation on the basis of our tectonic lineaments map.

### 3.5 Structural interpretation of gases and alteration

#### 3.5.1 Fracture segments in the distribution and concentration of gases

On Figures 8 and 9 we reported the gas concentration and distribution as measured by Gíslason et al. (1984) on top of our tectonic lineament map. The contour lines representing various gas measurements in steam coincide with sets of fractures as we mapped from aerial images.

- The most prominent set is the ENE, with sinistral and normal-slips. It appears controlling via 3 parallel fractures the ratio of H<sub>2</sub>/H<sub>2</sub>S, the concentration of H<sub>2</sub>S, and the distribution of oxygen isotopes (Figs. 8a to 8c). ENE fractures do not seem to have an effect in the concentration of chloride (Fig. 8d), but one major ENE fracture to the south of Tjarnarás Fault could play a role in the concentration of Radon (Fig. 8e). Often radon anomalies are considered as a precursor to earthquakes. Although micro-earthquakes from 1993 to 2011 do not show an apparent ENE alignment to the north of Bæjarfjall (Fig. 8f), Hjaltadóttir and Vogfjörð (2011) suggest that either a series of smaller NS dextral reverse-slip or a major ENE dextral reverse-slip fault could be the source of micro-earthquake

at depths of 3.5 to 7 km there. Our earlier structural analysis of these earthquakes indicate that an ENE sinistral fault is more likely to be the source fault of the micro-earthquakes, and the same fault is likely responsible for the ascent of radon (Fig. 8f). The ENE fractures could play minor role in the concentration of CO<sub>2</sub> (Fig. 9a), none in that of methane (Fig. 9b), and subtle influence in the heat distribution as determined from H<sub>2</sub>S, average gas temperature and CO<sub>2</sub> gas temperature (Figs. 9c to 9e).

- WNW set is the second most prominent fracture set strongly controlling the concentrations of chloride (Fig. 8d), CO<sub>2</sub> (Fig. 9a) and methane (Fig. 9b). The set also appears in the Ratio of H<sub>2</sub>/H<sub>2</sub>S (Fig. 8a), the concentrations of H<sub>2</sub>S (Fig. 8b), as well as the distribution of oxygen isotopes (Fig. 8c), and possibly the concentration of radon (Fig. 8e). The highest gas temperatures to the southwest of Ketilfjall also coincide with several parallel WNW fracture segments (Figs. 9c to 9e).
- The NW-NNW fractures, i.e., the dextral oblique-slip faults of Tjarnarás and a few adjacent parallel segments, appear strongly in the concentration of chloride (Fig. 8d), as well as the heat based on H<sub>2</sub>S (Fig. 9c) and the average gas temperatures (Fig. 9d). The NNW fracture segments appear to a lesser degree in the concentration of H<sub>2</sub>S (Fig. 8b) and the distribution of oxygen isotopes (Fig. 8c). But this set does not seem to influence the concentrations of Radon (Fig. 8e) and CO<sub>2</sub> (Fig. 9a), nor the CO<sub>2</sub> gas temperature (Fig. 9e). Some of these NW-NNW segments coincide also with the NW boundaries of gas provinces (Fig. 7i).
- The NNE sinistral oblique-slip fractures, particularly the segment to the southwest of Tjarnarás Fault, control the ratio of H<sub>2</sub>/H<sub>2</sub>S (Fig. 8a), the concentration of H<sub>2</sub>S (Fig. 8b), as well as the distributions of oxygen isotopes, chloride, CO<sub>2</sub>, and methane (Figs. 8c, 8d, 9a, 9b). The set also has apparent effect in the heat distribution as deduced from H<sub>2</sub>S (Fig. 9c), CO<sub>2</sub> (Fig. 9e) and the average gas temperature (Fig. 9d). The NNE set, however, has no obvious signature in the concentration of radon (Fig. 8e).
- The signature of a few shorter northerly rift-parallel segments is clear in the gases, particularly the open fractures and normal faults in the middle of Bæjarfjall and to the west of it. The most prominent influence of this set appears in the narrow northerly shape of the ratio of H<sub>2</sub>/H<sub>2</sub>S in the middle of Bæjarfjall (Fig. 8a). Otherwise, shorter northerly fracture segments coincide with the northerly elongation of the contours in the concentrations of H<sub>2</sub>S (Fig. 8b), Chloride (Fig. 8d), CO<sub>2</sub> (Fig. 9a), methane (Fig. 9b), as well as the distribution of oxygen isotopes (Fig. 8c). The set acts also in the temperature distribution of H<sub>2</sub>S, CO<sub>2</sub> and the average gas temperature (Figs. 9c, 9e, 9d), but has no role in the concentration of radon (Fig. 8e).
- The E-W set is the shortest and the least frequent of all sets and has a very subtle influence in the gases. Only one short E-W segment seems to have some influence in the Ratio of H<sub>2</sub>/H<sub>2</sub>S (Fig. 8a), as well as the concentrations of H<sub>2</sub>S (Fig. 9c) and Radon (Fig. 8e). Otherwise, the signature of this set is not seen in any other features of the gases.

### 3.5.2 Fracture segments influencing the gases and alterations

As surface alterations result from the circulation of geothermal fluids in rock matrix and fractures, a correlation between the structures controlling the gases and the alteration is critical.

The totality of the fractures interpreted as controlling the distribution and concentration of gases, as well as the gas temperatures are reported on the summary of the structures that we interpreted as being the weakest (Fig. 10a). The lineaments in the control of gases match perfectly the interpreted structural weak zones at Þeistareykir, Bæjarfjall and Tjarnarás. To reiterate, these sets are ENE, NE/ENE, WNW, NW-NNW, and to a lesser degree northerly and E-W.

For comparison, the fracture sets that we identified as controlling the surface geothermal alteration are reported on Fig. 10b, and on top of the weak zones. The same six sets of fractures are present. Based on aerial images observations of the fractures forming the weak zones as well as the analysis of their geometry, we concluded that all sets display apparent normal faulting. However, dextral motion is observed along some of the WNW and NW segments, and sinistral motion along a few of the NNE and ENE fractures. Although segments of the weak zones control the alteration locally, most of these structures belong to more regional fractures, which have greater length. The structural correlation of the gases and alteration indicate that (Fig. 10c):

- All the segments controlling the gases fall within the “alteration block” (Fig. 6a).
- The number of fractures dominating the gases is higher than those controlling the alteration. But the major faults responsible for the compartmentalisation of the alteration within the “alteration block” are the same as those controlling the gases. These are namely, the NW dextral oblique-slip Tjarnarás Fault, the WNW dextral strike-slip Stórhver Fault, the ENE sinistral segments to the north of Bæjarfjall on which a part of the micro-earthquakes occur, the NNE sinistral fault and a normal fault of the rift to the west of Bæjarfjall (Fig. 10c). These are the dominant structures in both the alteration and the gases, and a high number of fracture segments controlling the gases falls within these structures in the middle part of the “alteration block”.
- From this correlation it appears that the structures most favourable to fluid flow strike ENE, WNW and NW. The permeable fracture sets are thus the Riedel shear of the transform zone.

Although the depths from where gases ascend are indicative of the depth of the permeable host fractures, little evidence is at hand to deduce how deep the fracture sets or individual segments can be. Indication as to the depths of the fractures is further analysed in chapter 4.

### 3.6 Recall of the shift of Þeistareykir fissure swarm

In our preliminary analysis of the fracture pattern (Khodayar and Björnsson, 2013), we discussed briefly the shift of the Þeistareykir fissure swarm, which was for the first time pointed out by Gíslason et al (1984). The authors suggested that the Þeistareykir fissure

swarm is shifted to the west on a line from north of Tjarnarás to the north of Lambafjöll (Fig. 11a).

This shift has also been discussed by Sæmundsson (2007) and Sæmundsson et al. (2012a), who, based on the positions of the northern and southern grabens within the Þeistareykir swarm, estimate a 4 to 5 km displacement to the west along a WNW/NW line at Stórhver. Such a westward shift, however, implies existence of a sinistral motion along a WNW/NW fault, which would then have a horizontal motion opposite to the dextral motion along the WNW HFF.

A more thorough structural analysis on the geometry of faults in the central part of the Þeistareykir has been undertaken by Khodayar (2014). A model is suggested where the same exact shift is explained with a dextral motion across the WNW Stórhver Fault. Looking from the HFF to the south of Stórhver, the high number of normal faults concentrated on two opposite blocks across the Stórhver Fault indicates maximum extension compatible with the dextral motion of both HFF and Stórhver (Fig. 11b). Such deformation is similar to pull-apart basins on strike-slip faults.

We found it important to recall the results of Khodayar (2014) here, because they emphasise the importance of the WNW Stórhver Fault as one of the parallel structures within the transform zone and in the middle of the rift fissure swarm.

## 4 Sub-surface geophysical data

The 3D inversion of MT data by Karlsdóttir et al. (2012) is the most recent resistivity study in Þeistareykir and surroundings. Prior to the 3D inversion the MT data are corrected for static shift by joint inversion with TEM soundings at same locations. The 3D resistivity model of Þeistareykir geothermal field reflects both a conventional resistivity structure of a geothermal system as well as more regional features beyond the geothermal field. The main features in the resistivity are:

- A low resistivity cap, that reflects the zeolite/smectite alteration zone, covers the whole survey area. It reaches surface at Þeistareykir farm and dips down to 400–800 m (the upper limit) depth in all directions.
- A high resistivity core reflecting the chlorite/epidote alteration zone underlies the low resistivity cap. The margin between the two comprises the 230–240°C temperature boundary, provided that the alteration of the rock is in a thermal equilibrium within the geothermal system. The high resistivity core reaches highest under Þeistareykir to approximately 200 m b.s.l.
- Deep low resistivity bodies that may indicate the heat source and upflow zones of geothermal fluid into the system are the Ketilfjall anomaly and the Bæjarfjall anomalies and the Stórahversmór anomaly.
- In addition to the features connected to the geothermal field, two distinctive low resistivity bodies are present under the north western part of the survey area. They are connected to the low resistivity cap and reach down to 10 km b.s.l. It is

unknown whether their origin is alteration or magma. In their report, Karlsdóttir et al. (2012) interpreted these anomalies as being related to the TFZ.

The results of the resistivity model reveal the resistivity structures down to 12 km b.s.l. The TEM/MT data collection was carried out using a grid with sufficient data points (Fig. 12a). The location of inverted sections along parallel NS and EW lines are reported on Figs. 12b and 12c. Results are shown both as maps (Fig. 12d) and cross-sections (Figs. 12e and 12f). They indicate resistivity structures typical of a high temperature geothermal field from Ketilfjall to Peistareykir/Bóndhólsskarð. As stated above the data frame is more regional, indicating existence of a higher number of resistivity structures that overlap our tectonic lineaments map (Figs. 12g and 12h).

In spite of the fact that resolution of the MT method decreases with depth, results of the resistivity survey are reliable enough to identify structures with evident tectonic relevance. These structures are generally considered as mostly indicative of sub-surface alteration and fluid flow in geothermal fields.

Therefore, below we first interpret the resistivity structures from a structural point of view in order to better understand the tectonic control in sub-surface. Then we correlate the results with our identified surface fractures to obtain an idea about the depths of the fractures, and finally we make a brief correlation of the results with published gravimetry and magnetic data (Gíslason et al., 1984).

## **4.1 Tectonic control of the resistivity structures**

The low resistivity cap displays little structures on all cross-sections (e.g., Figs. 12e and 12f). However, deeper resistivity structures (more than 1000 m b.s.l.) have more obvious shapes (Figs. 13 to 23), and we emphasise on these latter in our interpretations.

### **4.1.1 A note on the width of the resistivity structures**

Before starting the structural analysis of the sub-surface data, we emphasise an important aspect, which is the width of the resistivity structures. The resistivity structures are of variable width, from less than 1 km to 4 km (Figs. 12e and 12f). On most of our figures, we interpret these structures as bounded by two faults. The reason for this interpretation is that we find it unlikely that structures of several hundred metres width are controlled by a single fault. Our understanding is based on field observations of a number of fault zones in rift contexts, which have been favourable to magma injection or to fluid flow resulting in geothermal alteration. As examples, in the Tertiary crust of Borgarfjörður in West Iceland, the width of altered fault zones injected by magma along single faults is up to 10 m width in Gljúfurá (Khodayar and Einarsson, 2002) and similar to the north of it (Khodayar et al., 2004). Occasionally, similar type of fault zones injected by dyke and highly altered can reach 40 m width, e.g., at Líkney in Hreppar microplate in South Iceland (Khodayar and Franzson, 2004). In the older geological context of Djibouti, the widest observed altered fault zone was up to 50 m (Khodayar, 2008). In most cases, the altered rocks are in the fault zone of oblique-slip faults.

The paleo burial depths of the rocks in which these fault zones were observed were 0.5 km in Hreppar microplate, 1.5 km in Borgarfjörður, and >2 km in Djibouti. It is unlikely that below 2–3 km, individual fault zone favourable to magma injection and

geothermal alteration reach several hundreds of metres width. Therefore, none of the resistivity structures interpreted here is considered to be controlled by a single fracture.

#### **4.1.2 Structural analysis of the resistivity data and correlation with fractures**

There are four supports shown on figures 13 to 23 as the ground for our structural analysis. All figures labelled as (a) are the original resistivity maps as shown in the work of Karlsdóttir et al. (2012). The figures labelled (b) are our structural interpretations of the resistivity structures where the lineaments controlling these bodies are drawn and their strikes shown in degree. The tectonic lineaments bounding these bodies are then superimposed on our overall surface fracture map labelled (c) and on the interpreted weak zones labelled (d) on all figures. We reiterate that the resistivity structures are organised along distinctive strikes and have en échelon geometries, which, similar to surface fractures, are indicative of strike-slip motions as discussed below. As all fracture sets have normal-slip, on figures labelled (b) we only show the sense of strike-slips along the tectonic lineaments controlling the resistivity structures.

We use mostly the low resistivity bodies under the high resistivity core in our structural interpretation as their geometries are more obvious at all depths, in particular from 1000 m b.s.l. downwards. We classify our interpretation of these structures according to the four depth ranges:

- *Depths of 0 and 500 m b.s.l.* The resistivity structures are numerous at 0 m where they are subtly bounded by series of WNW, ENE, NNW and short northerly lineaments (Fig. 13b). The traces of these lineaments coincide well with some of the mapped surface fractures from aerial photographs where WNW and NW fractures have dextral oblique-slip motions, ENE sinistral, and northerly fractures are rift-parallel and purely extensional (Figs. 13c and 13d).

The number of low resistivity structures decreases at 500 m b.s.l., while the tectonic pattern becomes clearer. The central area on the map around Stórhver (Fig. 14b) is highly resistive but without prominent geometries in the structures within the area. However, a few WNW, ENE and NW lineaments bound this high resistivity area (Fig. 14b). To the north, the low resistivity structures stretching from Sæluhúsveggur to the north of Ketilfjall begin to show the left-stepping en échelon arrangement typical of dextral motion on WNW structures. One ENE lineament could control the eastern edge of these structures to the north of Ketilfjall. Finally, two shorter NW and a couple of short northerly lineaments in the middle and southern part of the map bound the resistivity structures there. Although the lineaments deduced from 500 m b.s.l. are not always the same as those appearing at the depth of 0 m, they coincide well with other mapped fractures at the surface (Figs. 14c and 14d). A tectonic pattern already emerges from the depth of 500 m b.s.l. where the key process is the compartmentalisation along WNW, ENE, NW, and to a least degree along the northerly fracture sets.

- *Depth range of 1000 to 4000 m b.s.l.* A consistent tectonic configuration appears below the cap rock from 1000 to 4000 m b.s.l. (Figs. 15b to 20b). These are the depth-ranges of geothermal wells. Therefore, the interpretation of the structures at these depths is critical for the exploration and exploitation of the resource. From 1000 to



2000 m b.s.l. (Figs. 15a to 17a), the tectonic pattern is dominated by low resistivity bodies bounded by WNW zones to the north between Sæluhúsveggur and north of Stórhver, which extend farther east until north of Ketilfjall. Two WNW lineaments bounding the low resistivity bodies to the north range in strike from N114°E to N126°E and the lineaments themselves are in a left-stepping en échelon arrangement indicative of dextral motion. Within this WNW deformation band, several northerly lineaments coincide with the edges of local and shorter northerly low resistivity bodies. These bodies resemble smaller pull-apart structures associated with strike-slips. The lineaments bounding the resistivity structures farther east to the north of Ketilfjall range from NNE (N23°E) to ENE (N64°E). At the depths of 1500 and 2000 m b.s.l. to the northeast of Bæjarfjall, two ENE resistivity structures are obviously organised in right-stepping en échelon arrangement, indicative of sinistral motion along the ENE lineaments (Figs. 16b and 17b). Generally, some of the WNW and ENE lineaments at the depths of 1000 to 2000 m b.s.l. act also as the boundaries between the low resistivity structures to the north and the high resistivity area to the south of Stórhver (Figs. 15b to 17b).

The clear compartmentalisation seen at 1000 to 2000 m b.s.l. becomes even more detailed and with additional complexities from 2500 to 4000 m b.s.l. (Figs. 18b to 20b). The particular features emerging between 2500 and 4000 m b.s.l. are: (a) More low resistivity bodies appear to the south of Stórhver both at Hamrahlíð to the southwest and Bæjarfjall to the southeast; (b) To the north, the en échelon arrangements of the northerly and ENE low resistivity bodies within the NW and ENE bands become very distinct and strong. But from 3000 m b.s.l. the two ENE resistivity structures to the north of Bæjarfjall merge and become a single body; (c) The number of lineaments controlling the resistivity structures is higher at 2500 to 4000 m b.s.l. and there are slight changes in the strikes of the lineaments, i.e., the WNW / NW structures are in the range of N141°E at 2500 m b.s.l. but N155°E to N166°E at 4000 m b.s.l. The ENE structures range from N47°E to N50°E at 2500 m b.s.l. and from N61°E to N68°E at 4000 m b.s.l. (d) The northerly rift-parallel lineaments similar to pull-apart structures are always in the same locations within the WNW / NW deformation band to the north, and their strikes present the least variation. Only at 2500 m b.s.l. the tip of the easternmost northerly structure bends from N 10°E to N6°W (or N174°E in east quadrant). At 4000 m b.s.l. this small NW segment is clearly a part of a more regional NW lineament. (e) Convincing evidence of existence of E-W lineaments that control the resistivity bodies appears first at 4000 m b.s.l. at Kvíhólafjöll (Fig. 20b).

- *Depths of 5000 to 6000 m b.s.l.* The interesting features at these depths are: (a) Compared to the depth range of 4000 m b.s.l. there are fewer resistivity structures at 5000 m b.s.l. and even fewer at 6000 m b.s.l. (Figs. 21b and 22b). Whether this is due to a lesser resolution at those depths or indeed there are fewer structures cannot be determined from the data; (b) At 5000 m and 6000 m b.s.l. the resistivity structures appear within a distinct set of conjugate deformation bands controlled by WNW (N128°E) / NW (N149°E) and ENE (N50° to N86°E) lineaments. These values indicate a slight reversal in the strike of the structures compared to the depth range of 1000 to 4000 m b.s.l. (c) The northerly resistivity structures within

the WNW band are mostly bounded by NNE short lineaments, for which sinistral motion is deduced from our surface fractures. (d) The easternmost short northerly resistive structure to the north of Stórhver gradually merges with the ENE small resistivity structures to the north of Ketilfjall and Bæjarfjall, although a short northerly lineament could possibly control a small portion of this structure at Ketilfjall. (e) At 6000 m b.s.l. the ENE resistivity structures are sparse to the southwest of Tjarnarás Fault (Fig. 22b). To the north, the tectonic configuration is dominated by the conjugate WNW dextral and ENE sinistral deformation bands bounding the low resistivity structures. However, the northerly lineaments become more dominant to the west from Sandalda towards Stórhver, and there are two possible E-W lineaments controlling the structures to the south, i.e. east of Hamrahlíð and south of Kvíhólafjöll.

- *Depth of 8000 m b.s.l.* There are obvious changes in the number and the strikes of the structures at this depth compared to 5000 and 6000 m b.s.l. Four major structures dominate the depth of 8000 m b.s.l. (Fig. 23b): (a) The N-S zone from Sandalda to Stórhver is now well established and long, controlling distinct low-resistivity structures aligned N-S; (b) the WNW deformation zone is wider, stretching from Sæluhúsveggur to the south of Stórhver, and it is controlled by two sub-parallel lineaments striking N119°E and N105°E; (c) The ENE band, which formed a strong conjugate zone with the WNW lineaments at 5000 and 6000 m b.s.l. is still present in the same location, but the resistivity structure within the band is E-W and it is bounded by two E-W lineaments instead of ENE; (d) Only two small low resistivity structures exist, controlled by short parallel NW lineaments striking N152°E and N155°E (Fig. 23b).

The significance of these structures is discussed below, but it should be mentioned that at any depth, the lineaments emerging from the structural analysis of the resistivity structures fit well with specific sets of fractures mapped at the surface (Figs. 13c to 23d).

#### **4.1.3 Rotation in the tectonic structures and depths of the fractures**

The detailed structural analysis of the resistivity data shows a relevant but complex tectonic configuration, requiring explanations. Below, we suggest a simple mechanism leading to such complex tectonic configuration. Through this, we hope gaining insights into the relative depths and frequency of the fracture sets.

Side by side, we reported all of our structural interpretation of the resistivity structures on Maps 2a to 2i. We show the raw fracture map made from aerial images as guidance (Map 2j), but for clarity, we use the summary of the weak zones as a support for correlation with the fractures. We combined all of the interpreted lineaments from the resistivity structures from the depth of 1000 m b.s.l. to 4000 m b.s.l. on Map 2k, and helped with additional colours the interpretation of those depth-ranges on Map 2l. The lineaments from the depths of 5000 and 6000 m b.s.l. are grouped on Map 2m, and those of 8000 m b.s.l. on Map 2n. To reflect which structures are the weakest, we show also the results of the structural analysis of gases and alteration (Map 2o). For consistency, the rose diagram showing the strike-interval of each fracture set and their sense of motions

are plotted (Map 2p). Finally, we prepared a table summarising the detailed features related to the mechanism at the origin of the structures (Table 1).

From the above compilation, it appears that:

- The lineaments controlling the resistivity structures present a clockwise rotation between the depth of 1000 m b.s.l. and 4000 m b.s.l. (Maps 2a to f, 2k, 2l, and Table 1). Within this group, the amount of rotation including all fracture sets is between 20° and 43° E for this depth range, but most of it occurs at the depth of 2500 to 4000 m b.s.l. The dominant fractures sets within this depth range are WNW; ENE and NW, and secondarily northerly and NNE.
- The dominant lineaments controlling the resistivity structures at 5000 m b.s.l. are WNW to NW as well as ENE (Maps 2g, 2h, 2m), but at 6000 m b.s.l. five sets of lineaments play an equal role (ENE, WNW to NW; Northerly, NNE and E-W). The strikes of these structures are slightly different, indicating an anti-clockwise rotation of 6° to 19° to the west compared to the lineaments in the shallower depths of 1000 to 4000 m b.s.l. (Maps 2a and 2f; Table 1).
- At the depth of 8000 m b.s.l., the distinct tectonic configuration is dominated equally by four fracture sets (Northerly, E-W, WNW and NW), the strikes of which indicate again a clockwise rotation of 4° to 14° to the east compared to the depth range of 5000 to 6000 m b.s.l. (Map 2i, 2n, and Table 1).

From the above, one can suggest that the deepest structures are the four sets appearing at 8000 m b.s.l. with fewer lineaments but controlling more prominent resistivity structures. Among these, the E-W is the set that appears the last, i.e., from 4000 m b.s.l. downwards, and this may be the reason why there are so few E-W fractures at the surface. But fracturing is more numerous, mostly WNW/NW, ENE and NNE, particularly at depths of 2000 to 4000 m b.s.l.

**Table 1.** Summary of the fracture sets, their frequencies at each depth, the amount and sense of rotation.

Depths in (m) b.s.l	Fracture sets (highest frequencies marked in red)	Sense of rotation	Amount of rotation on fracture sets inside depth groups
0	WNW (N117°E to N 134°E) Northerly (N04° to N10°E) NW (N148°E to N158°E) ENE (N50°E to N59°E)		
500	WNW (N117°E to N 141°E) ENE (N66°E to N72°E) Northerly (N10°E to N11°E) NNE (N24°E)	Clockwise?	
1000	WNW (N114°E to N121°E) Northerly (N179°E to N05°E) NNE N17°E to N23°E) ENE (N64°E)	Clockwise	20°E to 43°E
1500	WNW (N118°E to N126°E) Northerly (N05°E to N07°E) NNE (N29°E to N31°E)	Clockwise	
2000	WNW (N114°E to N126°E) Northerly (N05°E to N07°E) NNE (N33°E to N35°E) ENE (N64°E) NW (N151°E)	Clockwise	
2500	ENE (N47°E to N50°E) NW (N141°E to N144°E) Northerly (N174°E to N11°E)	Clockwise	
3000	ENE (N56°E to N62°E) NW-NNW (N145°E to N155°E) Northerly (N10°E to N15°E) ENE (N21°E)	Clockwise	
4000	ENE (N61°E to N68°E) NNW (N152°E to N169°E) Northerly (N12°E to N16°E) NNE? (N19°E)	Clockwise	
5000	WNW to NW (N130°E to N149°E) ENE (N57°E to N83°E) Northerly (N10°E) NNE (N35°E) E-W (N91°E)	Anti-clockwise	6°W to 19°W
6000	ENE (N50°E to N86°E) WNW to NW (N128°E to N153°E) Northerly (N178°E) NNE (N28°E to N35°E) E-W (N90°E to N91°E)	Anti-clockwise	
8000	Northerly (N02°E) E-W (N89°E) WNW (N105°E to N119°E) NW (N153 to N155°E)	Clockwise	4° to 14°E

Three other considerations:

- A comparison between the structural analysis of the resistivity and that of the alteration and gases (Map 2o) is crucial. The ENE, NW WNW and NNE fractures determining the location of alteration and the distribution of gases match perfectly the lineaments controlling the resistivity structures in the same location. But these weak zones match best the lineaments seen in the resistivity structures that are at 2500 to 4000 m b.s.l., thus giving an indication of the major structures and their depths in resource exploitation. The depths of these fractures were unknown in our preliminary structural analysis given that the fractures were first identified on the ground of observations of aerial images (Khodayar and Björnsson, 2013). But with this present analysis, we have a relative depth and frequency of the fracture sets.
- The rose diagram on Map 2p is a recall of our interpretation of the sense of motion along fracture sets, as deduced from aerial images (Khodayar and Björnsson, 2013). These strike-intervals and motions are identical to the lineaments

controlling the resistivity structures, alteration and gases. They are also compatible with the direction of spreading at N105°E (DeMetz et al., 2010).

- And last, in a context where rift and transform segments act together, the role of the transform zone and its Riedel shears in the location and distribution of geothermal resources is as important as that of the rift.

## 4.2 Brief correlation with magnetic and gravity maps

A new gravity survey has been carried out by ÍSOR (Magnússon, 2011), but the results of the Bouguer map are not published yet. Therefore, for a brief correlation here, we use the earlier gravity and aeromagnetic maps from Gíslason et al., (1984). We reported on figures 24 to 26, respectively, the aeromagnetic, the Bouguer and the residual gravity maps from Gíslason et al. (1984). We then colored the contour intervals according to their values. The summary of the weak zones is superimposed on figures 24a, 25a and 26a, and the raw fractures on figures 24b, 25b and 26b. The blue colors in aeromagnetic data (Fig. 24a) represent the highest values (52000 to 53000 gamma) and likely correspond to regions of recent volcanism < 700.000 years with normal polarity (same polarity as the present-day magnetic field). Low values (50000 to 51000 gamma) are found to the north of Bæjarfjall, to the west and southwest of Skeiðin, and at Rauðhóll to the north. The magnetic low to the north of Bæjarfjall could be explained by geothermal alteration, destroying the magnetization of the rocks, but the other lows correspond to areas of older lavas with likely reverse polarity.

There is a general agreement between the Bouguer map (Fig. 25), and the residual Bouguer map (Fig. 26) on which the trend of the countrywide gravity bowl has been removed. The high values of the Bouguer (26 to 34 milligal) and the residual anomalies (3 to 5 milligal) are located to the west around Lambafjöll (northwest of Skeiðin and Hamrahlíð), as well as around Rauðhólar to the north of HFF within the fault system of TFZ. Gravity lows on the Bouguer (20 to < 26 milligal) and residual Bouguer (-3 to -7 milligal) maps cover three areas, namely north of Stórhver, east of Bóndhóll, and from south of Borgarhraun towards Stórhver. Gíslason et al. (1984) mention a “trough” when referring to the low and a “ridge” when referring to the high density rocks.

The magnetic highs and the gravity lows are bounded by older rocks with low magnetic and high gravity signatures. On regional scale, the magnetic highs and gravity lows are localised on the downthrown block of the HFF and can be edge effects from the faults of the TFZ (Figs. 24a, 25a, 26a). The reversely magnetised dense rocks dominate the northern flank of the TFZ, because either the young porous and normally magnetised rocks are eroded or they were never deposited there. But to the south of HFF (from Sandalda to Stórhver), the rocks have likely normal polarity but are less dense as they could be porous except in presence of dyke swarm or magmatic bodies.

Overall, the gravity and magnetic structures display WNW as well as northerly elongations. But in detail, the change in the value and shape of them coincide with WNW, NW, ENE, northerly, and to a least degree E-W tectonic lineaments that we mapped from aerial images (Figs. 24a to 26b). Almost the same major lineaments that emerged from the structural analysis of resistivity structures appear also in the gravity

and magnetic structures, the totality of which fits well with some of the weak zones we interpreted from surface mapping of fractures from aerial photographs.

## 5 Summary and Recommendations

In this Phase 2 of the structural analysis of Þeistareykir and surroundings, we made a new statistical analysis of the fracture map (Fig. 4) made by Khodayar and Björnsson (2013) and presented a new model explaining the shift of the northerly structures within the Þeistareykir fissure swarm (Fig. 11). The main focus of this study, however, was a multidisciplinary analysis of the tectonic control of alteration, gases, resistivity, aeromagnetics and gravity, and a correlation of the results with the fracture map mentioned above. All the data points to the same mechanisms at the junction of the Northern Rift Zone and the Tjörnes Fracture Zone:

1. We made a statistical analysis of fractures in three groups of rocks aged 2400 years, postglacial (from 8000 to 15000 years), as well as Quaternary and Upper Tertiary > 15000 years. The results show that fractures formed under the influence of the transform zone are present within the 2400 years lava, and only with time the effect of rifting becomes apparent in the postglacial series and older bedrock. Both the transform zone and the rift have critical roles in the development of fractures with time. The rift-parallel fractures in the rocks older than 8000 years are about 10%. The remaining sets belong to the Riedel shear of the transform zone (Fig. 4).
2. The same results appear in the tectonic control of the location and distribution of alteration (Fig. 6), and gases (Figs. 8 to 10). This suggests that the geothermal activity is dominantly controlled by the Riedel shears of the transform zone and secondarily by the rift.
3. As one of the Riedel shears, the WNW dextral strike-slip fault of Stórhver-Bæjarfjall, parallel to the HFF, has a great influence on geothermal activity and is also likely responsible for the 2400 years old eruption within the fissure swarm. The dextral motion along the WNW Stórhver-Bæjarfjall Fault led to maximum stretching on the blocks that moved dextral and resulted in two northerly pull-apart structures similar to classical pull-apart “basins” and a high number of normal faults on those blocks (Fig. 11b).
4. The structural interpretation of the resistivity bodies shows a gradual clockwise rotation up to 40°E of these structures from 1000 to 4000 m b.s.l. (Figs. 15 to 20, Map 2). In these depth ranges, the resistivity structures display strong en échelon geometries and seem to be controlled by WNW to NW dextral, and NNE to NE sinistral tectonic lineaments. A small portion of the structures strikes northerly and their geometry within the WNW deformation band appears similar to pull-apart structures associated with strike-slips (Map 2). An anti-clock rotation of the resistivity structures appears to occur at 5000 and 6000 m b.s.l. where the same Riedel shears dominate but the strikes of the lineaments are clearly shifted 4° to 16° W (Figs. 21 and 22, Map 2). At the depth of 8000 m b.s.l. (Fig. 23, Map 2), most of the resistivity structures have either merged or the resolution of the MT at that

depth is not enough to distinguish the structures in more details. However, a few major structures seem present, controlled equally by a few N-S, E-W, WNW and NNW lineaments. Among all of the sets, E-W appears deepest, i.e., from 4000 m b.s.l. down. That could explain why there are so few and faint E-W fractures expressed at the surface (Figs. 3c, 4c to 4e, 10).

5. The northerly strike of the rift and the WNW strike of the main transform fault are dominant in the gravity and magnetic structures (Figs. 24 to 26). But in detail all of the Riedel shears identified from the surface fractures appear at the sub-surface and coincide with changes in the values and shape of contour lines of magnetic and gravity structures. The E-W set is the least frequent also among these data.

Two main results should be kept in mind from our multidisciplinary analysis:

- (a) Almost the same weak structural zones appear to control a variety of processes ranging from fracturing, geothermal activity, alteration, eruption, and even the shape of the resistivity bodies at the surface and sub-surface.
- (b) The rift and the E-W structures seem to have a crucial role in the deformation at a greater depth, i.e., 8000 m b.s.l. and possibly below. The Riedel shears of the transform zone on the other hand are, not only the most frequent set of fractures, but they control most of the resources and geological processes in the upper 8 km in the crust.

All the critical details relevant to well siting and drilling could not be addressed here due to limited framework of Phase 2. Therefore, we recommend that the following be carried out during the Phase 3 of the structural analysis to shed more light on the structures identified in this phase:

1. Report the dip-slips of all fractures on the summary results, and check the major horsts and grabens that may appear through this complement.
2. Compare more thoroughly the specific lineaments that appear between data types, and prepare a final map with all these structures.
3. Check the depths of the most relevant fractures by correlation with borehole data (a major task).
4. Obtain the newest published gravity maps by ÍSOR and correlate them with the fracture map.

It should be emphasised that Phase 2 brought a step forward in unravelling the overall tectonic control in Peistareykir and surrounding. But the above recommendations for Phase 3 will help identifying with greater certainties the permeable fractures for drilling.

**Acknowledgments.** This report is prepared for Landsvirkjun. Our special thanks go to Ásgrímur Guðmundsson and Egill Júlíusson at Landsvirkjun for their support and project management. At ÍSOR, we wish to thank the following colleagues, Magnús Ólafsson for his excellent management of this project; Sigurður Garðar Kristinsson for his constructive review of the report; Guðrún S. Jónsdóttir, Gunnlaugur M. Einarsson, and Skúli Víkingsson for their help with GIS issues; Finnbogi Óskarsson and Halldór Ármannsson for discussions on geochemistry of gases; and Hrafnhildur Harðardóttir for her efforts to edit the report.

## 6 References

- Ármansson, H. (2004). Chemical aspects of exploration of the Þeistareykir high-temperature geothermal area, N-E Iceland. *Water-Rock interaction*, 63–67. Eds.: R. B. Wanty and R. R. Seal II. Taylor and Francis Group, London.
- Ármansson, H., Kristmannsdóttir, H., Torfason, H., and Ólafsson, M. (2000). Natural changes in unexploited high-temperature geothermal areas in Iceland. *Proc. World Geothermal Congress 2000*, 521–526.
- DeMets, C., Gordon, R. G., and Argus, D. F. (2010). Geologically current plate motions. *Geophysical Journal International*, 181 (1), 1–80.
- Einarsson, P. (1979). Seismicity and earthquake focal mechanisms along the mid-Atlantic plate boundary between Iceland and the Azores. *Tectonophysics*, 55, 127–153.
- Einarsson, P. (1991). Earthquakes and present-day tectonism in Iceland. *Tectonophysics*, 189, 261–279.
- Einarsson, P., and Björnsson, S. (1979). Earthquakes in Iceland, *Jökull*, 29, 37–43.
- Garcia, S., Angelier, J., Bergerat, F., and Homberg, C. (2002). Tectonic analysis of an oceanic transform fault zone based on fault-slip data and earthquake focal mechanisms: the Húsavík-Flatey Fault zone, Iceland. *Tectonophysics*, 344, 157–174.
- Geirsson, H., Árnadóttir, Th., Hreinsdóttir, S., Decriem, J., LaFemina, P. C., Jónsson, S., Bennett, R. A., Metzger, S., Holland, A., Sturkell, E., Villemin, T., Völksen, C., Sigmundsson, F., Einarsson, P., Roberts, M. J., and Sveinbjörnsson, H. (2010). Overview of results from continuous GPS observations in Iceland from 1995 to 2010. *Jökull*, 60, 3–22.
- Gíslason, G., Johnsen, G. V., Ármansson, H., Torfason, H., and Árnason, K. (1984). *Þeistareykir: Yfirborðsrannsóknir á háhitasvæðinu*. National Energy Authority, report, OS-84089/JHD-16, 134 p. and 3 maps.
- Guðmundsson, A., Gautason, B., Lacasse, Ch., Axelsson, G., Þorgilsson, G., Ármansson, H., Tulinius, H., Sæmundsson, K., Karlsdóttir, R., Kjaran, S. P., Pálmarrsson, S. Ó., Halldórsdóttir, S., and Egilson, P. (2008). *Hugmyndalíkan jarðhitakerfisins á Þeistareykjum og jarðvarmamát með rúmmálsaðferð*. Iceland GeoSurvey, report, ÍSOR-2008/024, MV-049 and Vatnaskil 08.05, 67 p.
- Halldórsson, P. (2005). *Jarðskjálftavirkni á Norðurlandi - Earthquake activity in N-Iceland*. Veðurstofa Íslands, IMO report 05021, 34 p.
- Hjaltadóttir, S., and Vogfjörð, K. (2011). *Sprungukortlagning við Þeistareyki og Bjarnarflag með háupplausnarstaðsetningum smáskjálfta*. Landsvirkjun, report, LV-2011-116, 44 p.
- Hermannsson, S., and Línadal, B. (1951). *Efnagreining á hverum og laugum*. Jarðboranir ríkisins.
- Jakobsdóttir, S. S. (2008). Seismicity in Iceland: 1994–2007. *Jökull*, 58, 75–100.



- Jancin, M., Young, K. D., Voight, B., Aronson, J. L., and Sæmundsson, K. (1985). Stratigraphy and K/Ar ages across the west flank of the Northeast Iceland axial rift zone, in relation to the 7 Ma volcano-tectonic reorganization of Iceland. *Journal of Geophysical Research*, 90, 9961–9985.
- Karlsdóttir, R., Vilhjálmsson, A. M., Árnason, K., and Teklesenbet Beyene, A. (2012). *Peistareykir Geothermal Area, Northern Iceland: 3D Inversion of MT and TEM Data*. Iceland GeoSurvey, report, ÍSOR-2012/046, 173 p. + CD.
- Khodayar, M. (2008). *Results of the 2007 surface geothermal exploration in the Asal Rift and Transform zones, Djibouti: Tectonics and Geothermal manifestations*. Iceland GeoSurvey, report, ÍSOR-2008/008, 70 p.
- Khodayar, M. (2014). *Shift of Peistareykir fissure swarm in Tjörnes Fracture Zone: Case of pull-apart on strike-slip?* Iceland GeoSurvey, report, ÍSOR-2014/074, LV-2014-144, 21 p.
- Khodayar, M., and Björnsson, S. (2013). *Preliminary Fracture Analysis of Peistareykir geothermal field and surroundings, Northern Rift Zone and Tjörnes Fracture Zone*. Iceland GeoSurvey, ÍSOR-2013/029. 57 p., 2 maps.
- Khodayar, M., and Einarsson, P. (2002). Strike-slip faulting, normal faulting, and lateral dike injections along a single fault: Field example of the Gljúfurá fault near a Tertiary oblique rift-transform zone, Borgarfjörður, west Iceland. *Journal of geophysical research*, vol. 107, NO. B5, 10.1029/2001JB000150, 2002. 16 p.
- Khodayar, M., and Franzson, H. (2004). *Stratigraphy and tectonics of eastern Núpur/western Hagafjall in Gnúpverjahreppur, South Iceland*. Iceland GeoSurvey, report, ÍSOR-2004/017. 42 p.
- Khodayar, M., and Víkingsson, S. (2015). *Note on determining the fracture frequency in the statistical analysis of large fracture populations*. Iceland GeoSurvey, short report, ÍSOR-15016, 8 p.
- Khodayar, M., Franzson, H., Björnsson, S., Víkingsson, S. and Jónsdóttir, G. S. (2004). *Tectonic lineaments of Borgarfjörður–Hvalfjörður from aerial photographs, West Iceland: Preliminary results*. Iceland GeoSurvey, report, ÍSOR-2004/021. 48 p.
- Kristinsson, S. G., Friðriksson, Þ., Ólafsson, M., Gunnarsdóttir, S. H., and Nielsson, S. (2013a). *Háhitavæðin á Peistareykjum, í Kröflu og Námafjalli. Vöktun á yfirborðsvirkni og grunnvatni*. Iceland GeoSurvey, ÍSOR-2013/037, LV-2013-091, 152 p.
- Kristinsson, S. G., Óskarsson, F., Ólafsson, M., Óladóttir, A. A., Tryggvason, H., H., og Friðriksson, Þ. (2013b). *Háhitavæðin í Námafjalli, Kröflu og á Peistareykjum. Vöktun á yfirborðsvirkni og grunnvatni árið 2013*. Iceland GeoSurvey, ÍSOR-2013/060, LV-2013-132, 160 p.
- Mamula, N., and Voight, B. (1985). Tectonic analysis of lineaments near spreading axis, Northeastern Iceland. *Tectonophysics*, 116, 63–93.
- Magnúsdóttir, S., and Brandsdóttir, B. (2011). Tectonics of Peistareykir fissure swarm. *Jökull*, 61, 65–79.
- Magnússon, I. Þ. (2011). *Þyngdarmælingar á Peistareykjum í ágúst 2011*. Iceland GeoSurvey, report, ÍSOR-2011/081, 15 p. + appendices.

- Óskarsson, F. (2011). *Háhitaholur á Þeistareykjum. Efnasamsetning vökva og gufu*. Iceland GeoSurvey, report, ÍSOR-2011/068, 28 p.
- Rögnvaldsson, S. T., Gudmundsson, A., and Slunga, R. (1998). Seismotectonic analysis of the Tjörnes Fracture Zone, an active transform fault in north Iceland. *Journal of Geophysical Research*, 103, 30117–30129.
- Stefánsson, R., Guðmundsson, G. B., and Halldórsson, P. (2008). Tjörnes fracture zone. New and old seismic evidences for the link between the North Iceland rift zone and the Mid-Atlantic ridge. *Tectonophysics*, 447, 117–126.
- Sæmundsson, K. (1978). Fissure swarms and central volcanoes of the neovolcanic zones of Iceland. *Geological Journal, Special Issue*, 10, 415–432.
- Sæmundsson, K. (2007). *Jarðfræðin á Þeistareykjum*. Iceland GeoSurvey, short report, ÍSOR-07270, 23 p.
- Sæmundsson, K., Sigurgeirsson, M. Á., and Grönvold, K. (2012a). *Þeistareykir. Jarðfræðirannsóknir 2011*. Iceland GeoSurvey, report, ÍSOR-2012/024, 61 p., with map.
- Sæmundsson, K., Hjartarson, Á., Kaldal, I., Sigurgeirsson, M. Á., Kristinsson, S. G., and Víkingsson, S. (2012b). *Geological Map of Northern Volcanic Zone, Iceland. Northern part. 1:100.000*. Reykjavík, Iceland GeoSurvey and Landsvirkjun.
- Voight, B., and Mamula, N. Jr. (1983). Structures and tectonics of northern Iceland. In J. E. Estes and G.A. (edits) *Thorley Manual of Remote Sensing, 2nd ed., Vol. 2.*, 1782–1786, American Society of Photogrammetry, Falls Church, Va.
- Young, K. D., Jancin, M., Voight, B., and Orkan, N. I. (1985). Transform deformation of Tertiary rocks along the Tjörnes Fracture Zone, North Central Iceland. *Journal of Geophysical Research*, 90, 9986–10,010.

## Figures

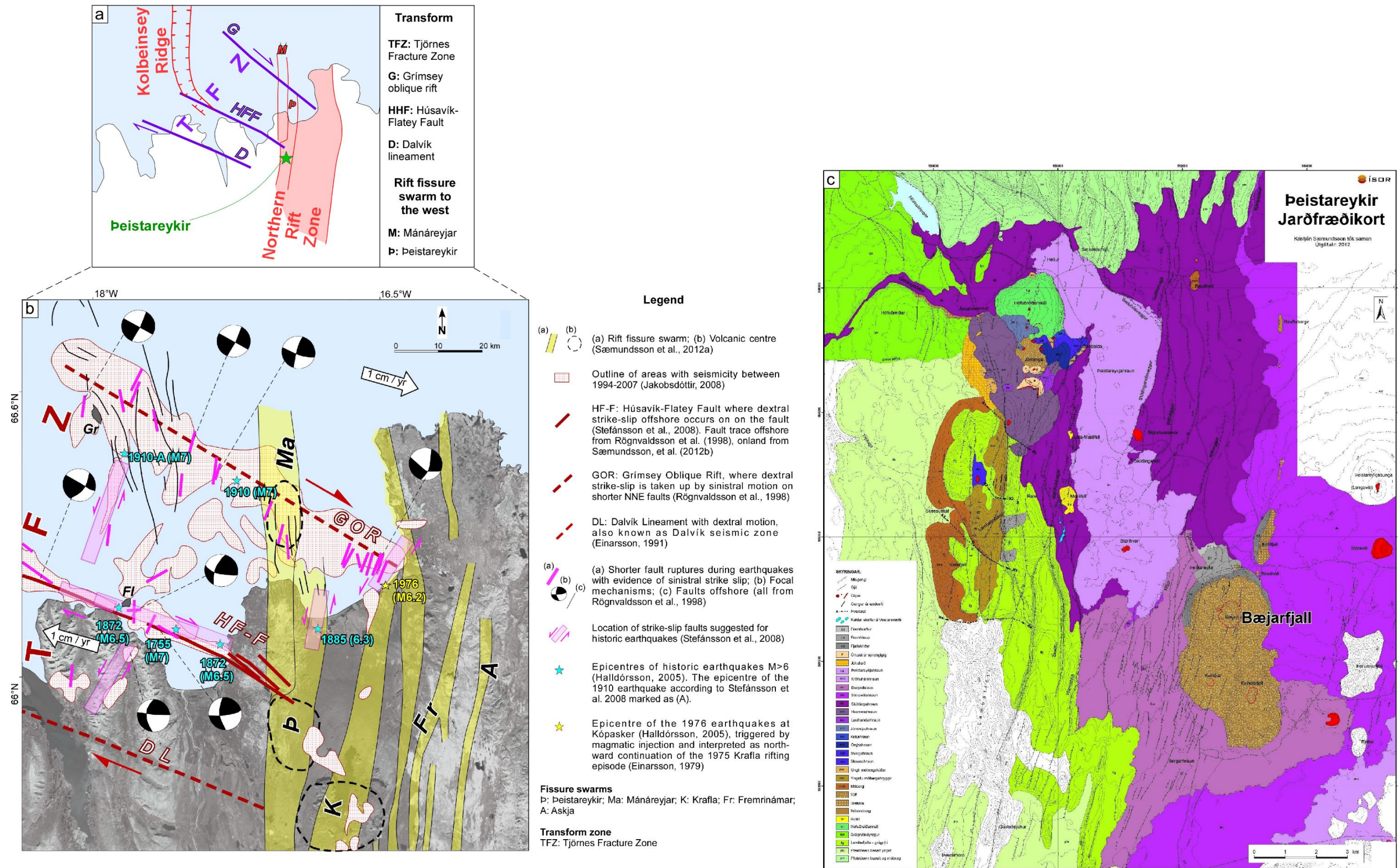


**Figure 1.** Overview of geological context. (a) Location of Peistareykir geothermal field at the junction of Northern Rift Zone and Tjörnes Fracture Zone. (b) Compilation of tectonic elements of the rift and the transform zones plate boundaries in North Iceland. (c) Geological map by Sæmundsson et al. (2012b) emphasizing rift parallel fractures.

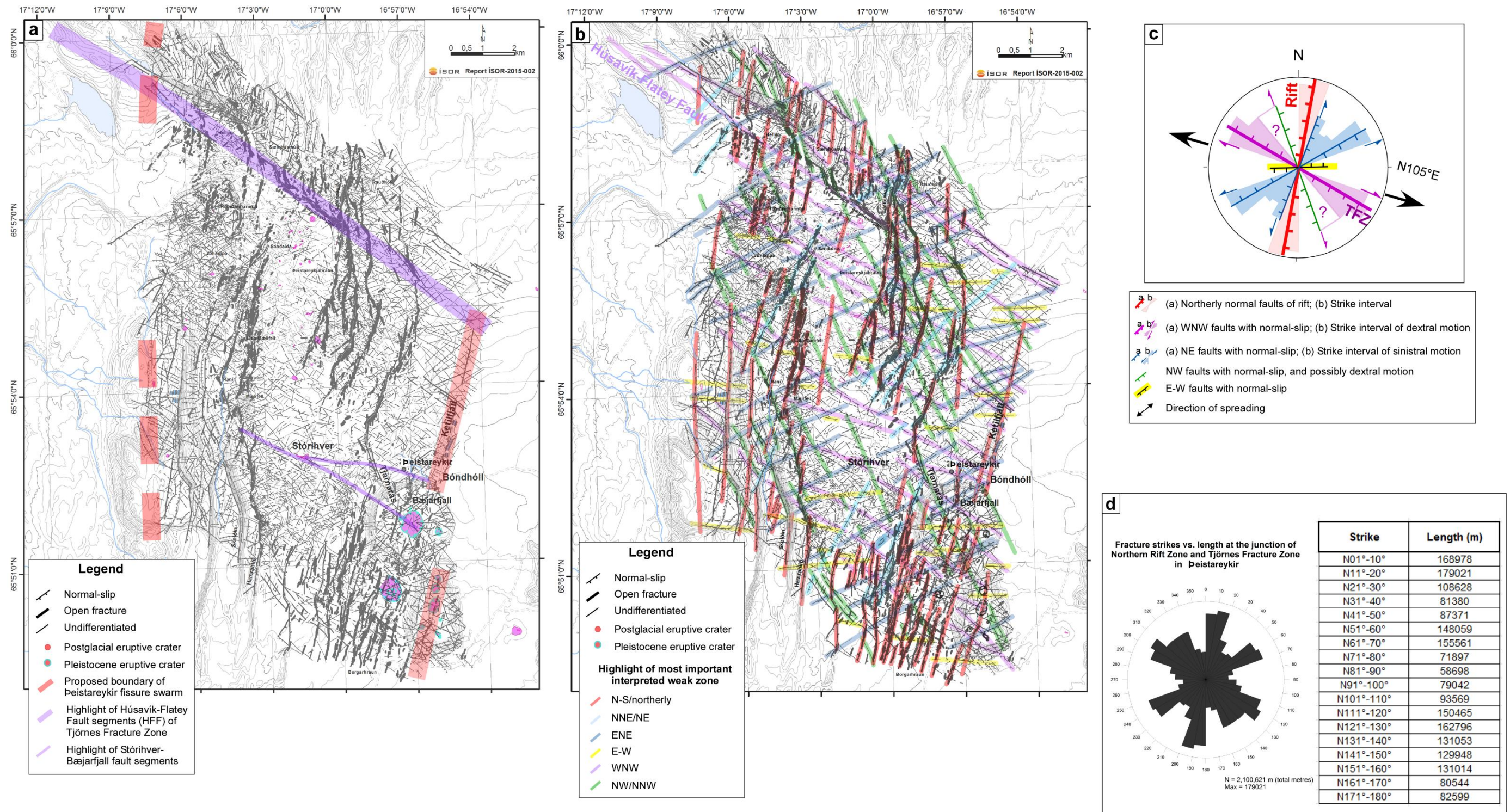


**Figure 2.** Recall of some results from Phase 1 of structural analysis of Peistareykir (Modified from Khodayar and Björnsson, 2013). (a) Tectonic pattern interpreted from observation of aerial images showing traces and types of major and minor fracture segments. The boundary of the Peistareykir fissure swarm, the Húsavík-Flatey Fault of the Tjörnes transform zone, and the WNW Stórihver-Bæjarfjall Fault are highlighted. (b) Six sets of fractures and highlight of the interpreted structural weak zones. (c) Rose diagram showing the strike-interval and motions along the fracture sets, reflecting the combination of extensional rift-parallel fractures and the Riedel shears of the transform zone. (d) Recall of the preliminary statistical analysis of the fracture population (total of 10729 segments) with the most frequent strikes.

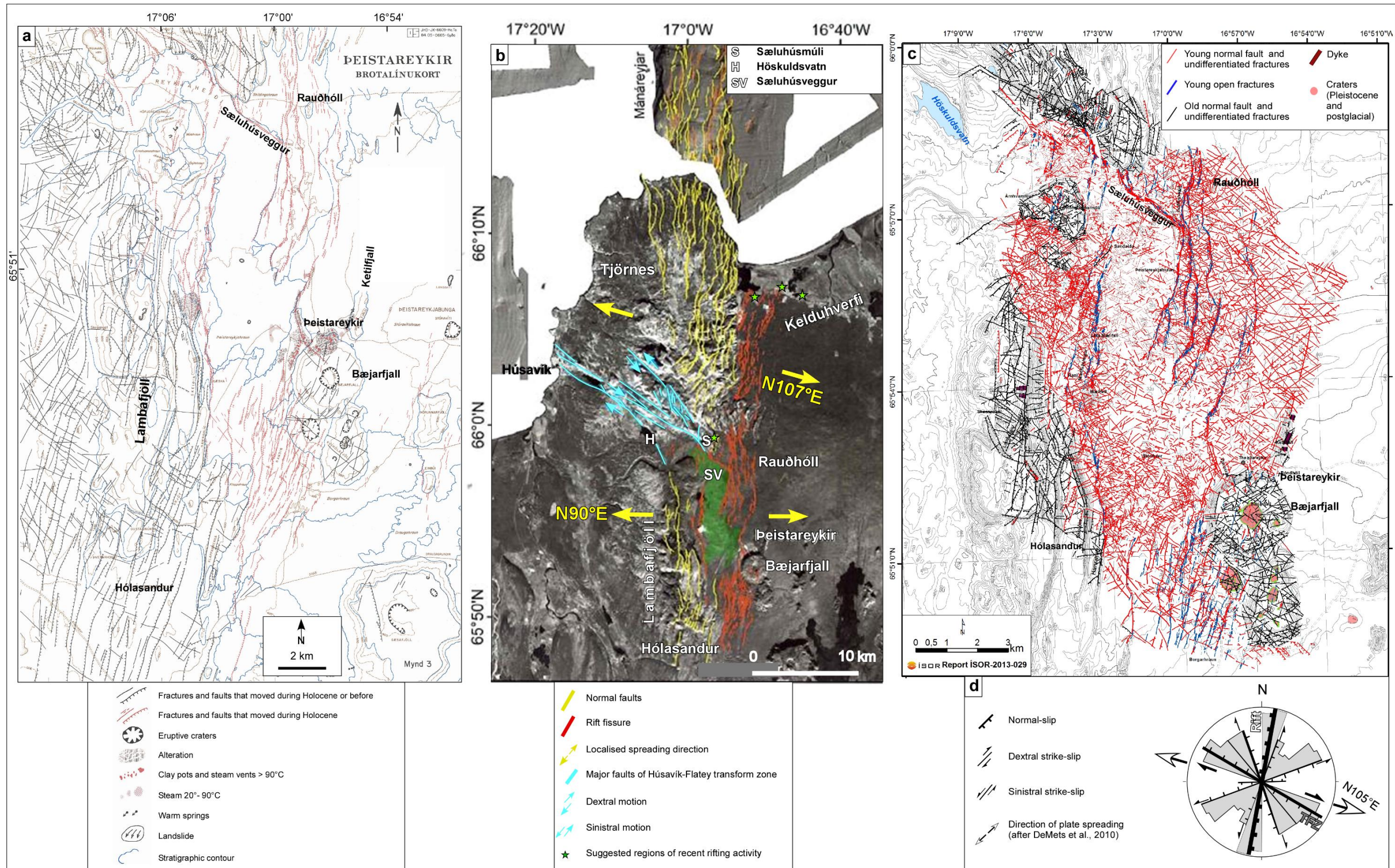


**Figure 3.** Correlation of our tectonic lineament map with previous structural maps also made from images. (a) Tectonic lineament map of Gíslason et al. (1984) made mostly from pairs of aerial photographs. (b) Tectonic lineament map made from spot and aerial images onshore and bathymetric images offshore (Magnúsdóttir and Brandsdóttir, 2011). (c) Tectonic lineament map from three types of aerial images (pairs of aerial photographs, 3 bands of Spot5 satellite image, two bands of orthomaps from 1998 and 2007) where fractures are identified based on relative age, types, and traces (Khodayar and Björnsson, 2013). (d) Rose diagram of the strike-intervals and motions along the observed sets of fractures belonging to rift and transform on figure (c). See text for correlation and further explanations.

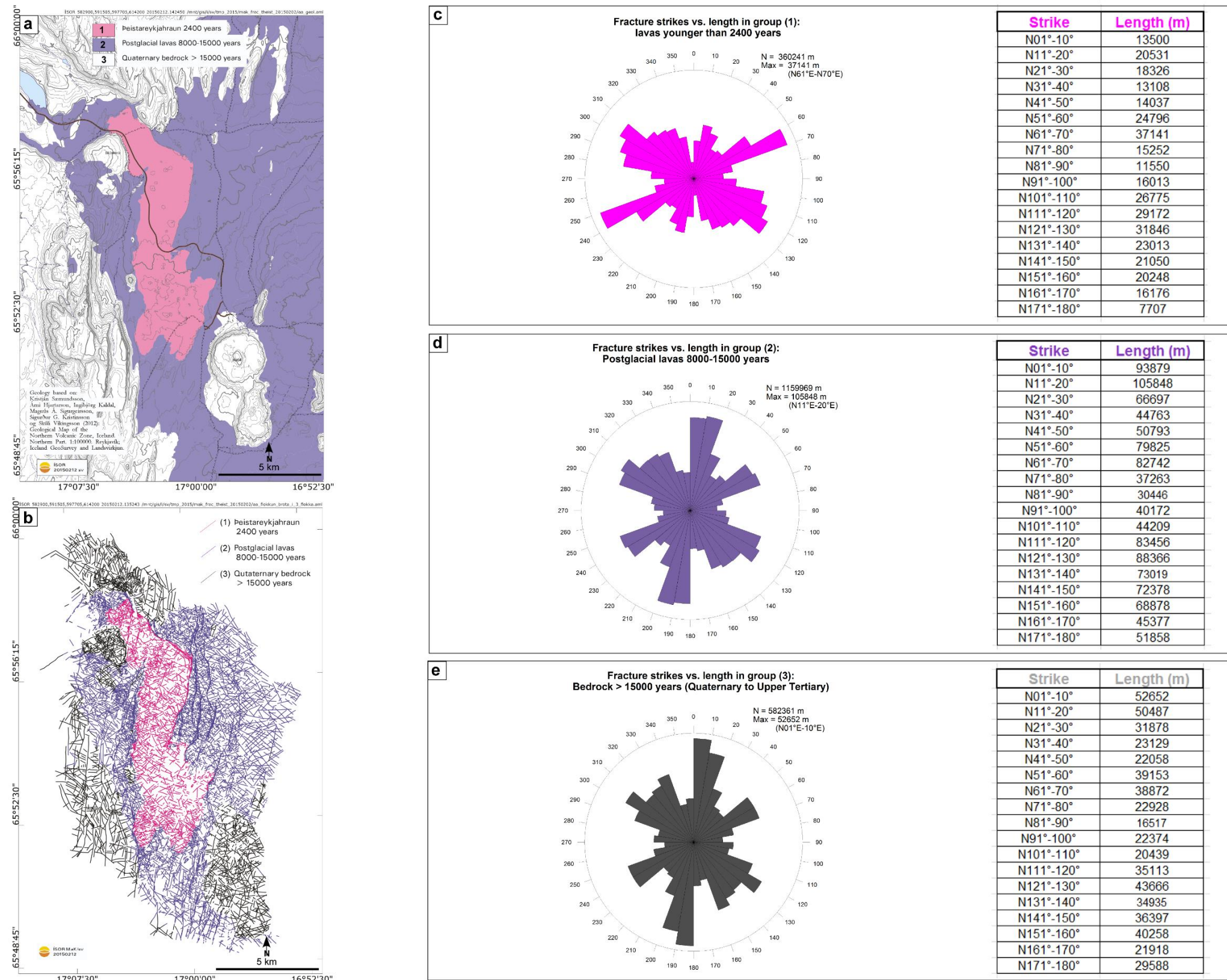


**Figure 4.** Statistical analysis per relative age of the fractures interpreted from aerial images by Khodayar and Björnsson (2013). (a) Geological map of Sæmundsson et al., (2012b) simplified in three groups of relative rock ages, used as support for the statistical analysis. (b) Fractures from Khodayar and Björnsson (2013) divided into three groups according to the relative rock ages on figure (a). Figures (c) (d) and (e) Rose diagrams and tables showing, respectively, the strikes of the most frequent fractures in the 2400 years old Peistareykir lava, the postglacial lavas (8000-15000 years old series, and the bedrock > 15000 years old (Quaternary to Upper Tertiary).

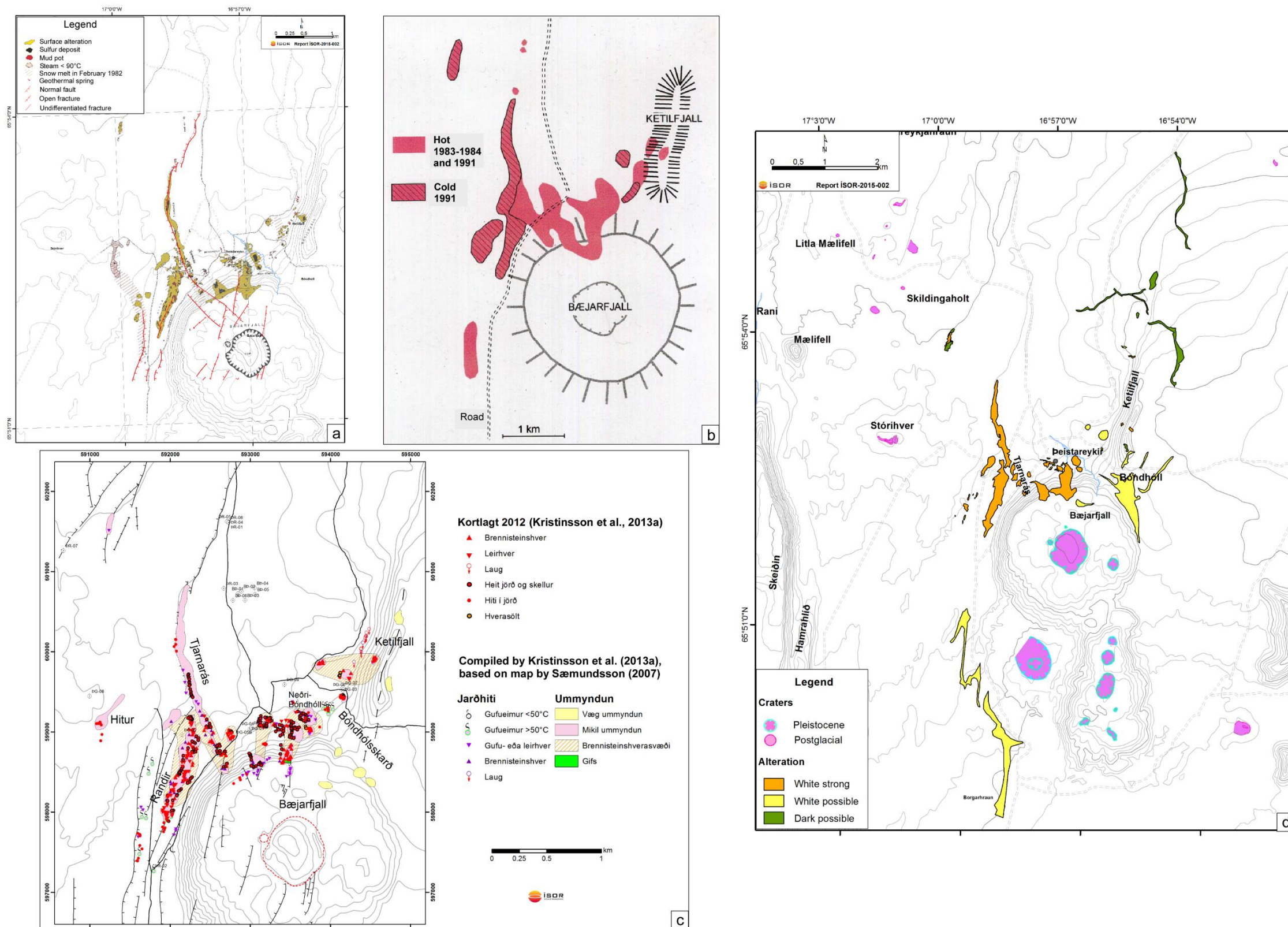


**Figure 5.** The mapped alteration in Tjarnarás, Bæjarfjall, Ketilfjall and Deistareykir in the field and from aerial images. (a) Alteration and surrounding faults mapped by Gíslason et al. (1984). (b) Simplified alteration and indication of change in temperature between 1984 and 1991 (Ármansson et al., 2000). (c) Newest map of alteration and geothermal springs at Deistareykir (Kristinsson et al., 2013a). (d) Surface geothermal alteration mapped from aerial images in this study.



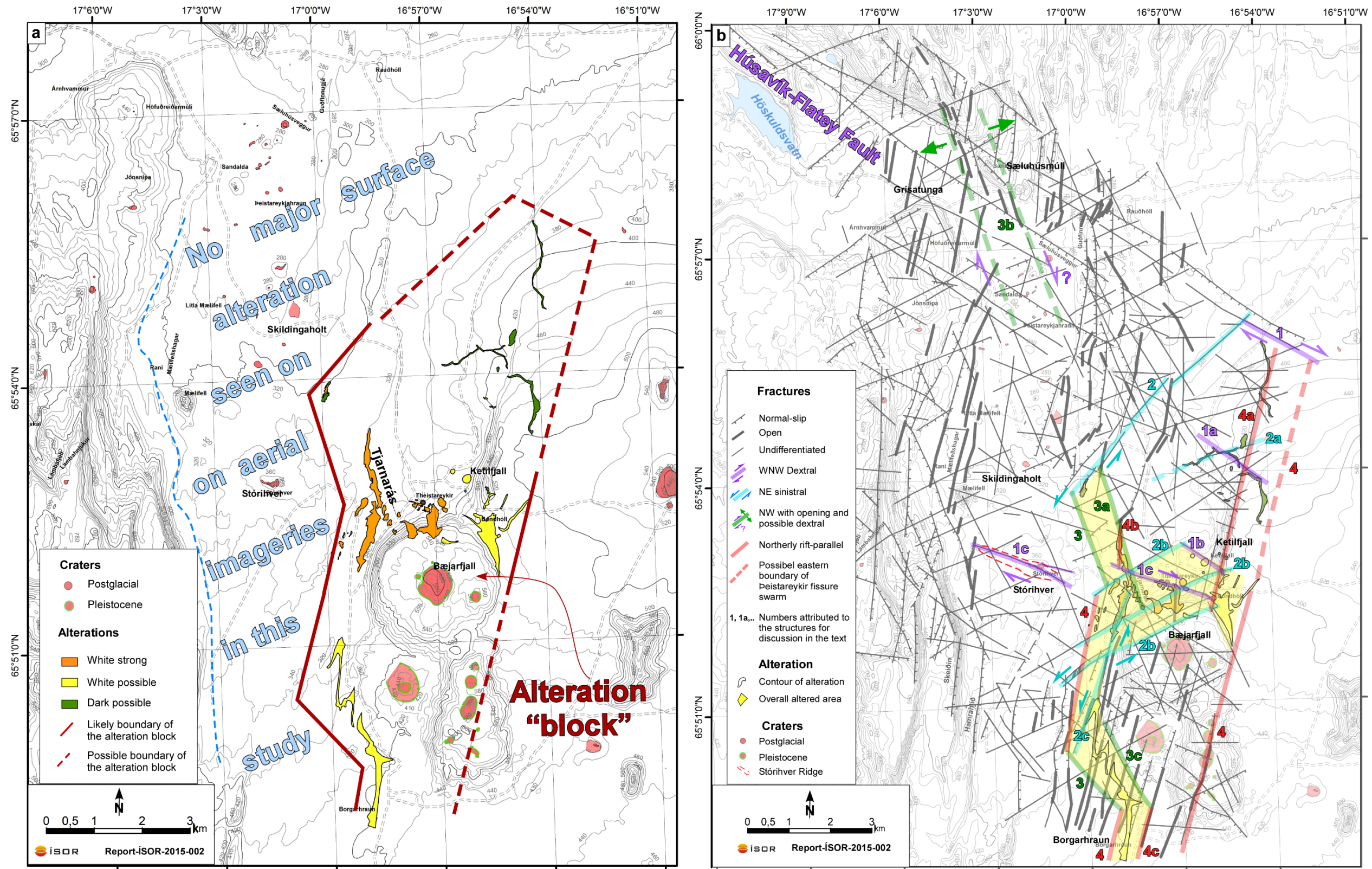


**Figure 6.** Location and tectonic control of alteration in Deistareykir and immediate surroundings. (a) Suggested boundaries of the alteration block. (b) Boundaries and location of the alteration within the alteration block compared to interpreted weak zones. See text for explanation.

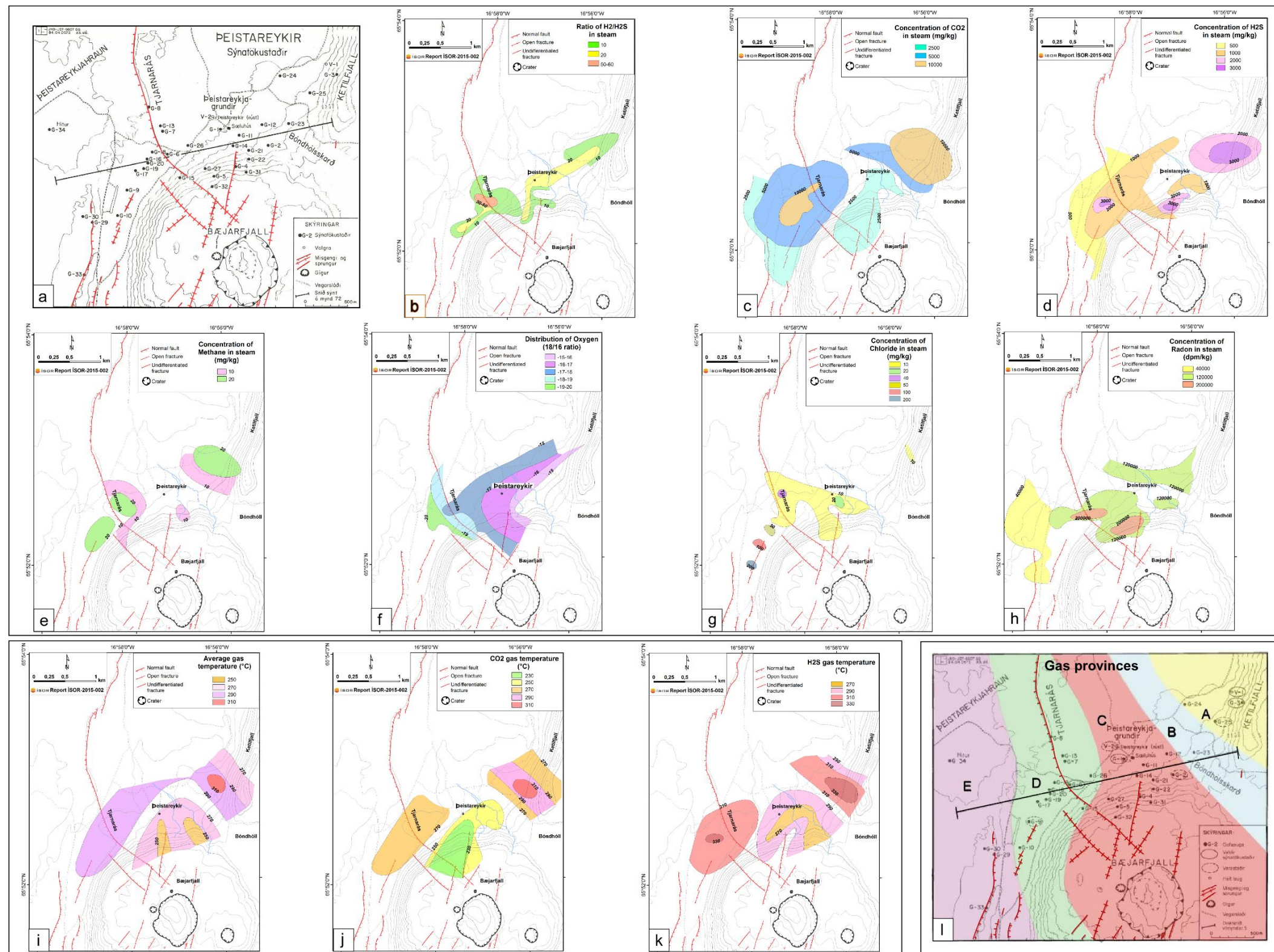


**Figure 7.** Concentration, distribution, ratio of geochemical elements in steam, and gas provinces at Peistareykir. (a) Data points where Gíslason et al. (1984) collected data to plot figures (b) to (k). Figures (b) to (k) from Gíslason et al. (1984) show respectively the status of H<sub>2</sub>/H<sub>2</sub>S, CO<sub>2</sub>, H<sub>2</sub>S, methane, <sup>18</sup>O/<sup>16</sup>O, chloride, radon, as well as average gas temperature, CO<sub>2</sub> gas temperature, and H<sub>2</sub>S gas temperature. (l) Gas provinces as suggested by Gíslason et al. (1984) and Guðmundsson et al. (2008).

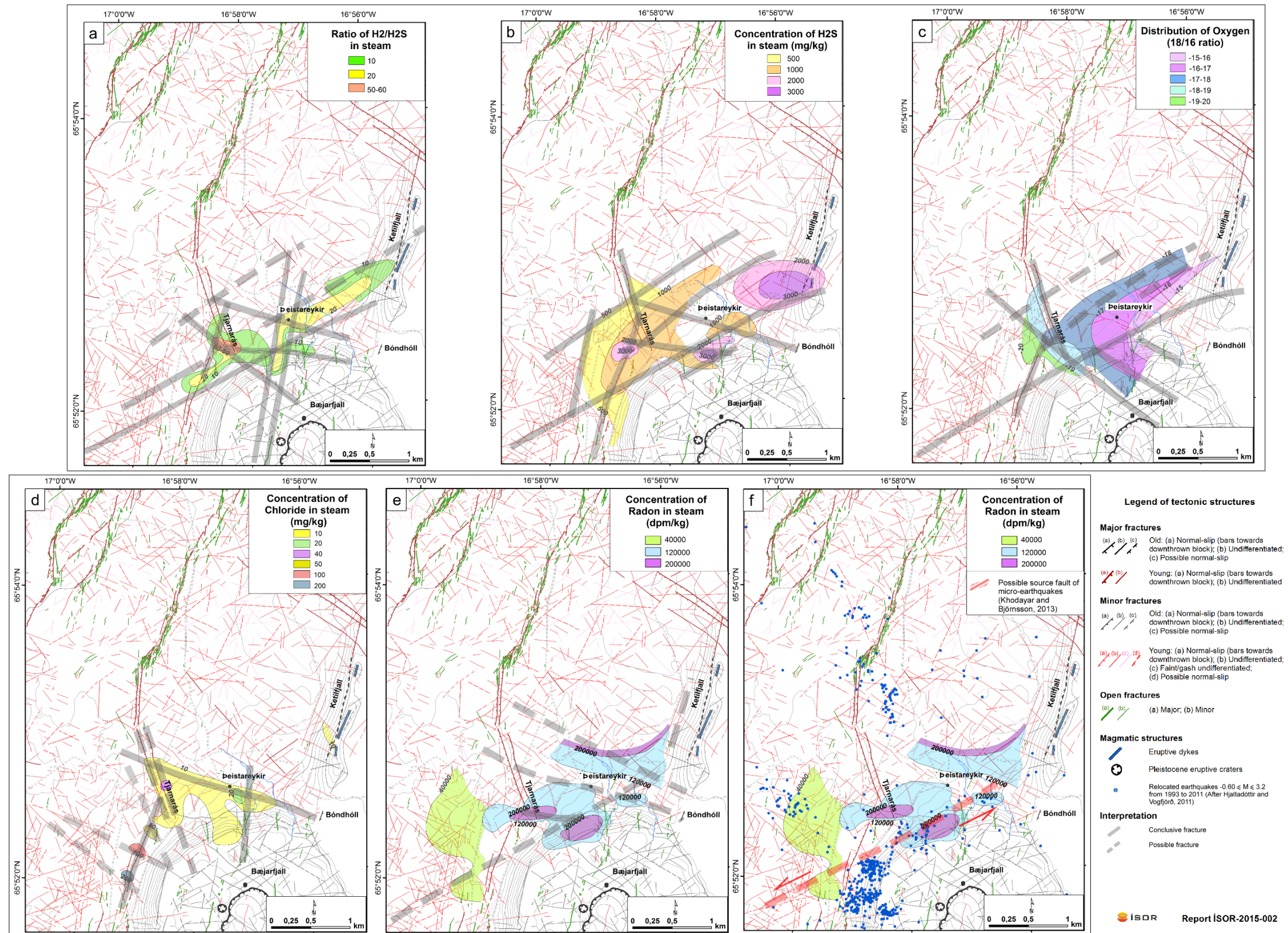


**Figure 8.** Our tectonic interpretation of the concentration, distribution, and ratio of geochemical elements in steam at Peistareykir. (a) Ratio  $H_2/H_2S$  controlled dominantly by ENE, then by WNW and northerly lineaments. (b) and (c) Concentrations of  $H_2S$  and distribution of  $^{18}O/^{16}O$  along the same lineaments as on figure (a). (d) Concentration of chloride dominated by ENE, NE and northerly fractures. (e) Concentration of radon primarily dominated by WNW and ENE, and secondarily by E-W and possibly northerly structures. (f) Correlation with the concentration of radon and micro-earthquakes 1993-2011 shows no plausible correlation except for an ENE sinistral fracture north of Bæjarfjall.

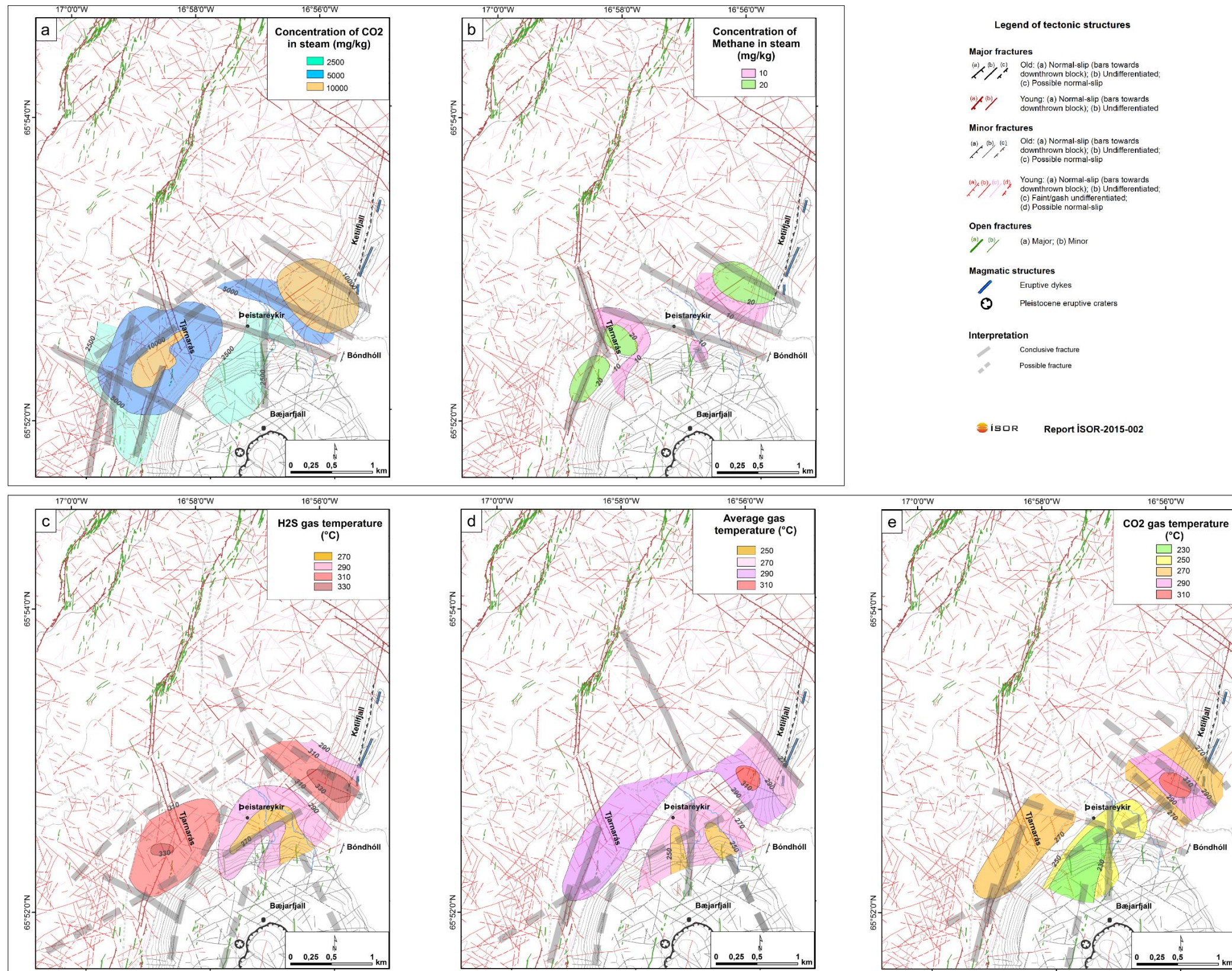


**Figure 9.** Our tectonic interpretation of the concentration of geochemical elements in steam as well as the gas temperatures at Beistareykir. (a) Concentration of CO<sub>2</sub> controlled by WNW, northerly and ENE tectonic lineaments. (b) Concentration of radon controlled by ENE, NNW and northerly lineaments. (c) to (e) Respectively, H<sub>2</sub>S gas temperature, average gas temperature, and CO<sub>2</sub> gas temperature dominantly controlled by ENE and WNW, and secondarily by NNW and northerly/NNE lineaments.

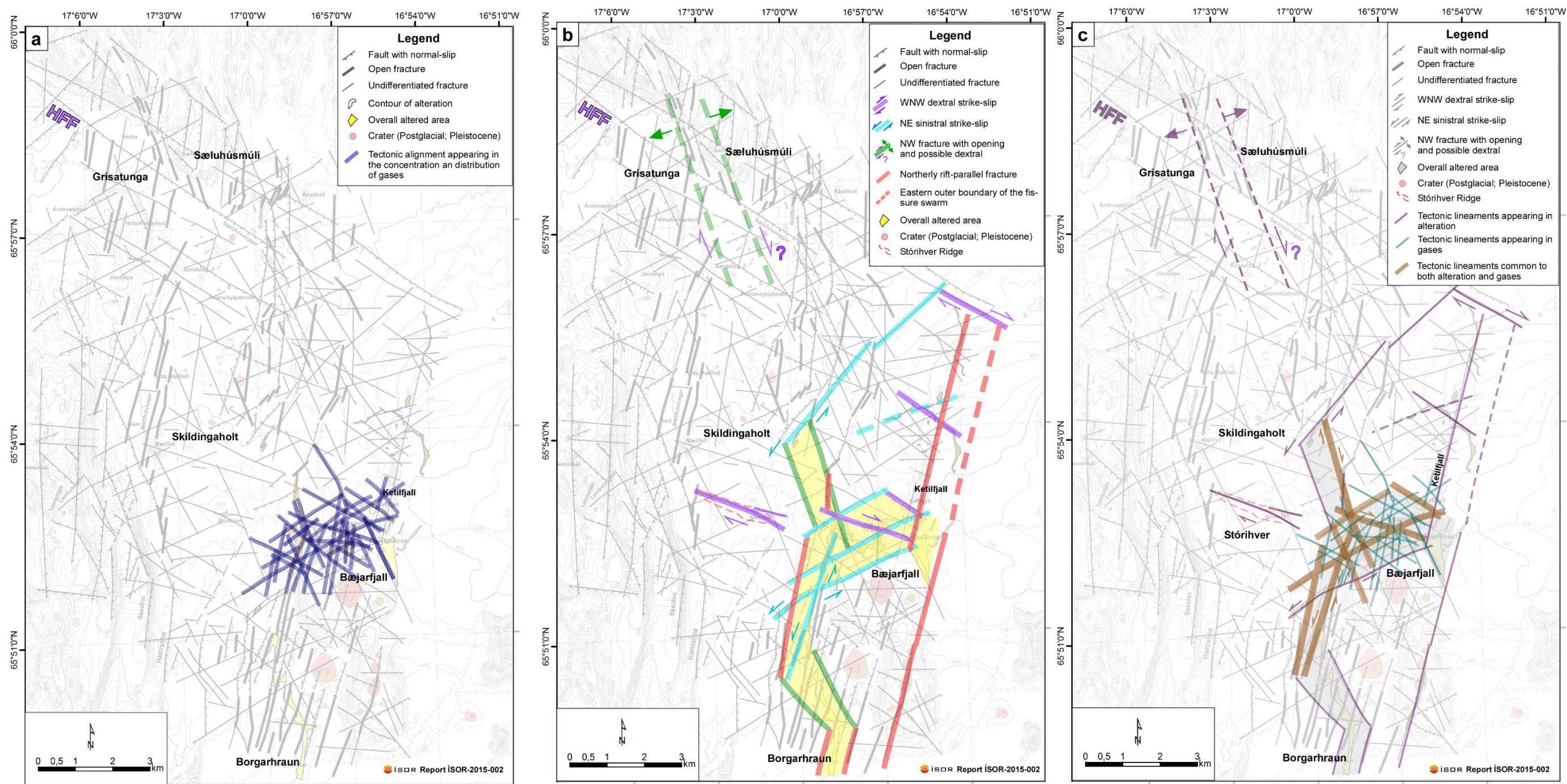


**Figure 10.** Correlation between lineaments emerging from tectonic interpretation of gases, alteration, and interpreted weak zones. (a) Compilation of lineaments seen in the distribution, concentration of gases as well as gas temperatures. (b) Suggested lineaments controlling the alteration block and the alteration within it. (c) Compilation of the lineaments seen in gases and alteration and the weak zones. Note that the same ENE, NNE, NNW and a few WNW fractures are common to all of these processes.

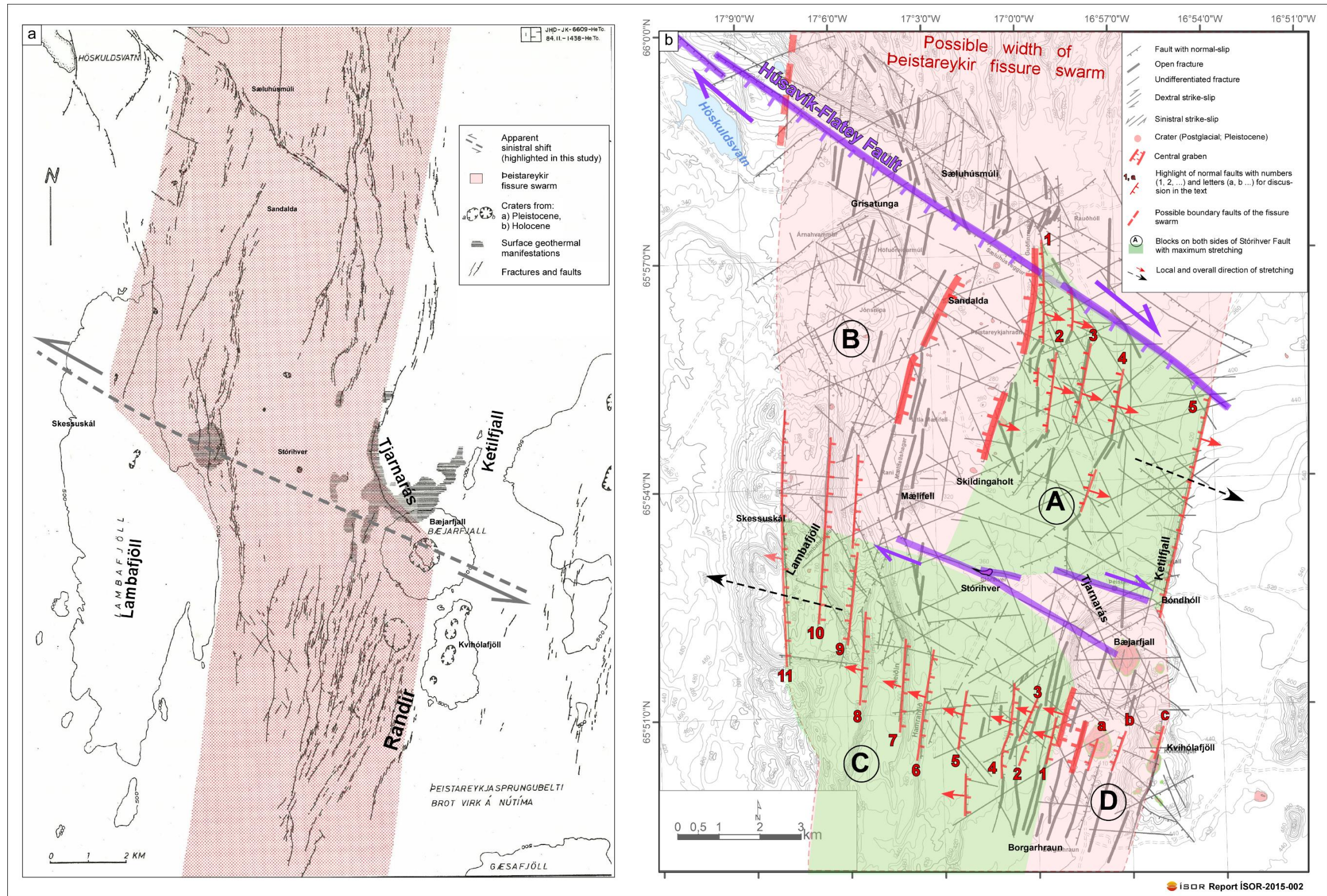


**Figure 11.** New explanation as to the mechanism responsible for the shift of the structures in the Peistareykir fissure swarm. (a) The shift of the Peistareykir swarm as initially suggested by Gíslason et al. (1984) requires existence of a WNW sinistral strike-slip from Tjarnarás to the north of Lambafjöll. (b) Alternative for the shift of the grabens requiring a dextral strike-slip fault at the latitude of Bæjarfjall-Stórihver in the Peistareykir fissure swarm (Khodayar, 2014). Note that the blocks (A) and (C) bear the highest number of normal faults, and blocks (B) and (D) the lowest. Concentration of normal faults in these blocks is supportive of maximum stretching and extension, compatible with the dextral motion of the WNW Bæjarfjall-Stórihver Fault.

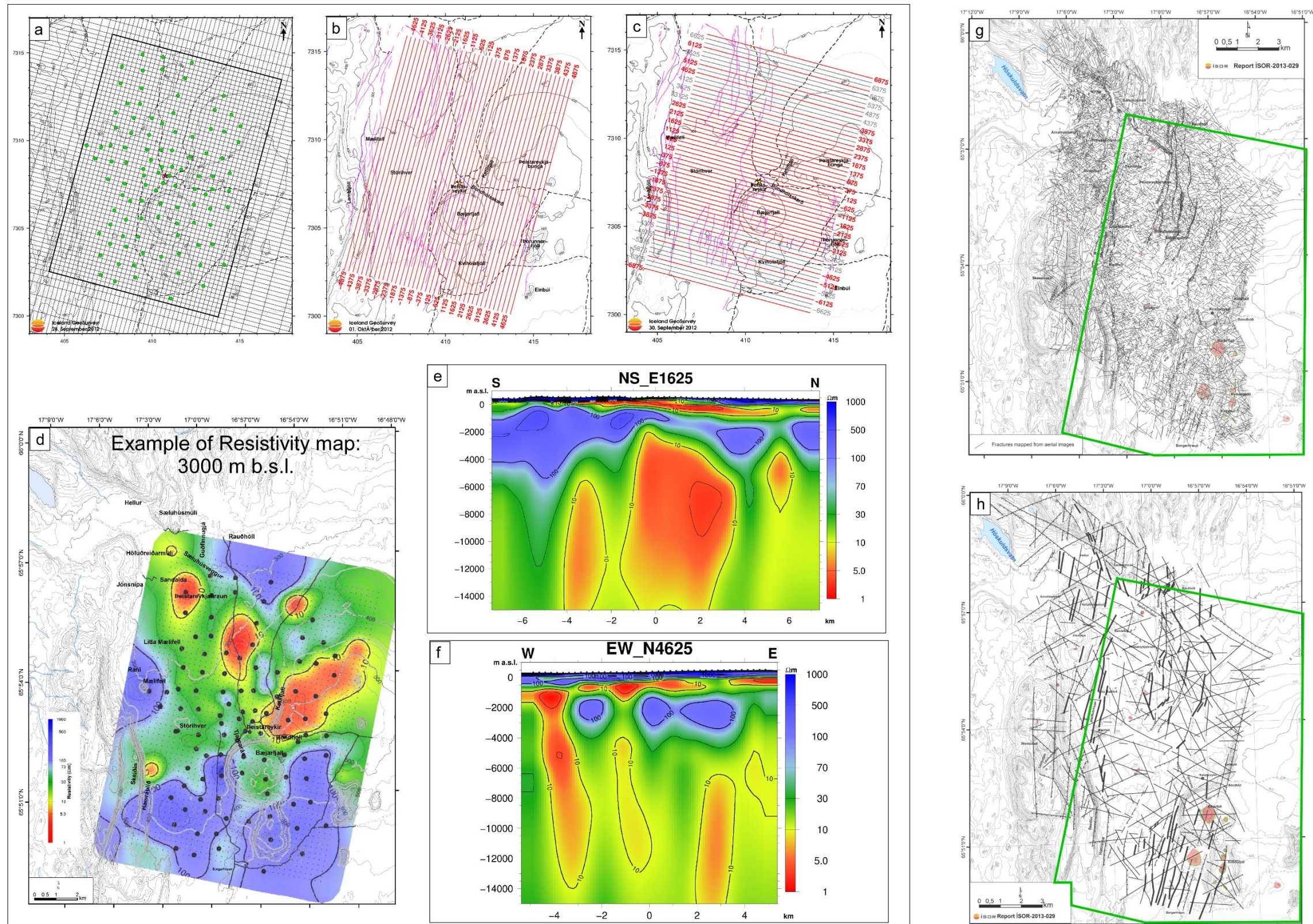


**Figure 12.** Frame of TEM/MT survey compared to the fracture map, and type of results showing the resistivity structures. (a) to (c) Data points and the grid used by Karlsdóttir et al. (2012) for TEM/MT survey. (d) Example of 3D inversion of MT resistivity structures shown as map. (e) and (f) Example of 3D inversion of MT resistivity structures shown in cross-sections. (g) and (h) respectively, frame of MT data superimposed on the overall fracture map and interpreted weak zones by Khodayar and Björnsson (2013).

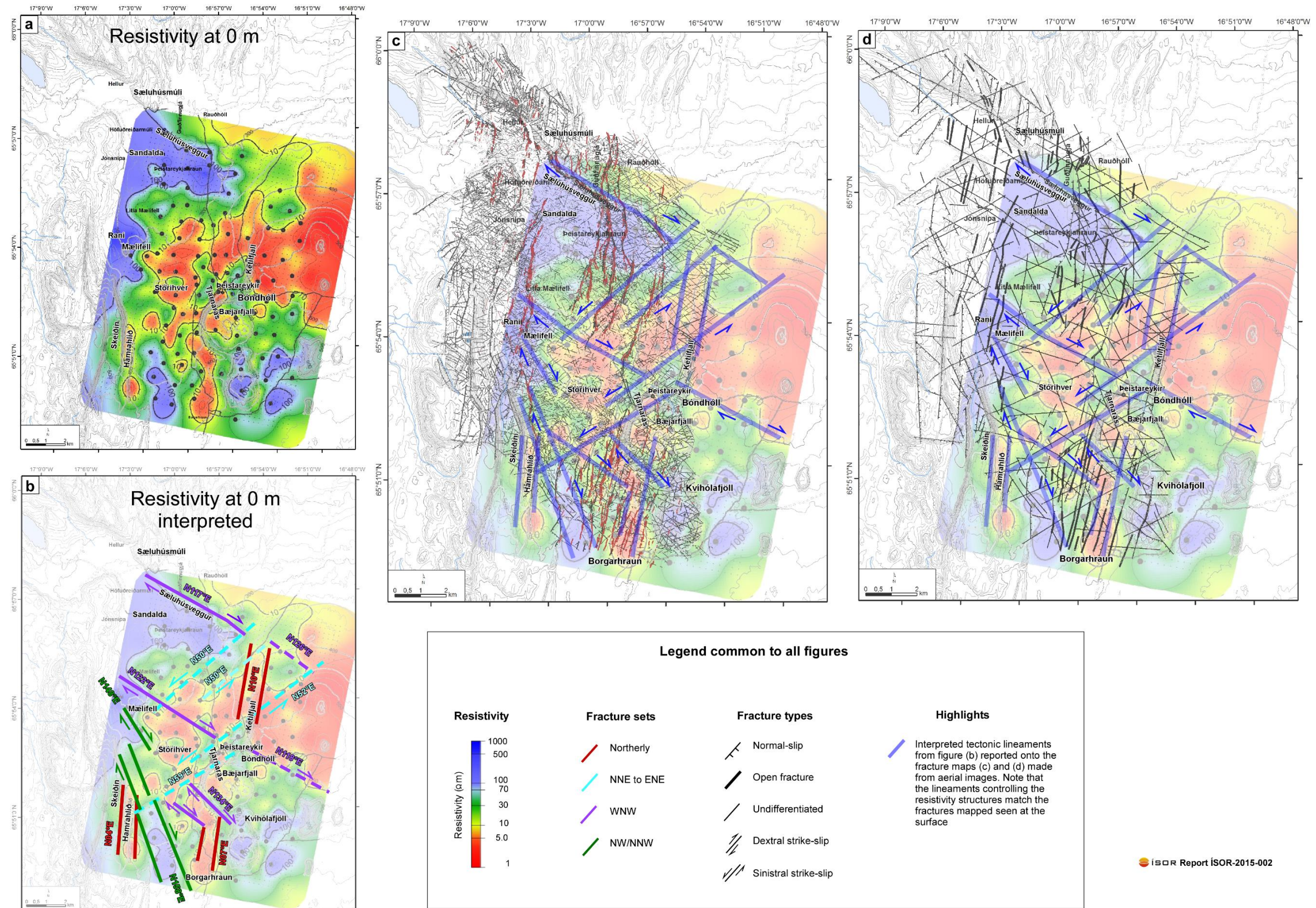


**Figure 13.** Structural interpretation of the resistivity structures at 0 m. (a) Un-interpreted resistivity map of Karlsdóttir et al. (2012) at 0 m. (b) Our structural interpretation of the resistivity structures. The interpreted lineaments from the resistivity structures superimposed on: (c) the fracture map, and (d) the interpreted weak zones by Khodayar and Björnsson (2013).



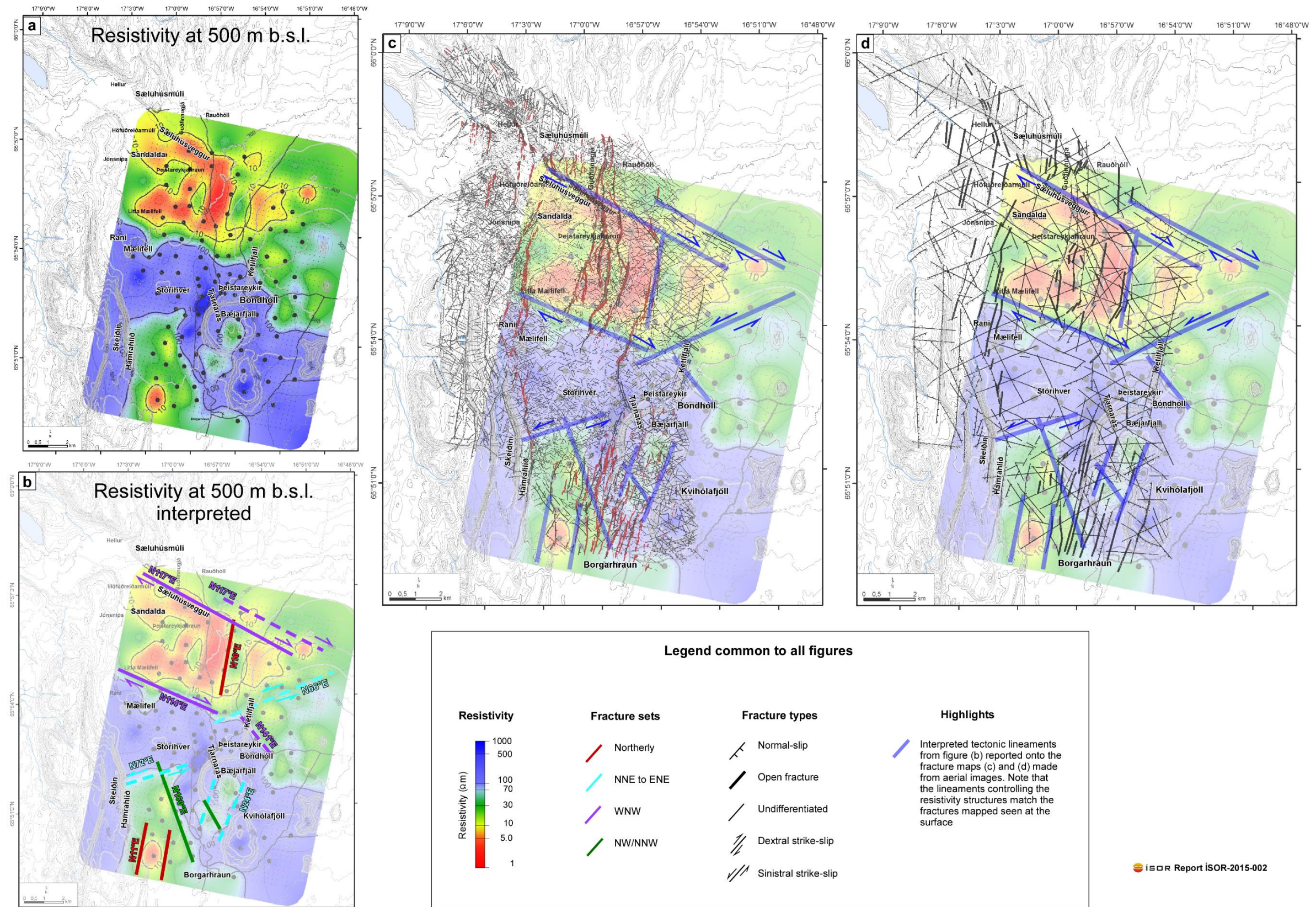


**Figure 14.** Structural interpretation of the resistivity structures at 500 m b.s.l. (a) Un-interpreted resistivity map of Karlsdóttir et al. (2012) at 500 m b.s.l. (b) Our structural interpretation of the resistivity structures. The interpreted lineaments from the resistivity structures superimposed on: (c) the fracture map, and (d) the interpreted weak zones by Khodayar and Björnsson (2013).

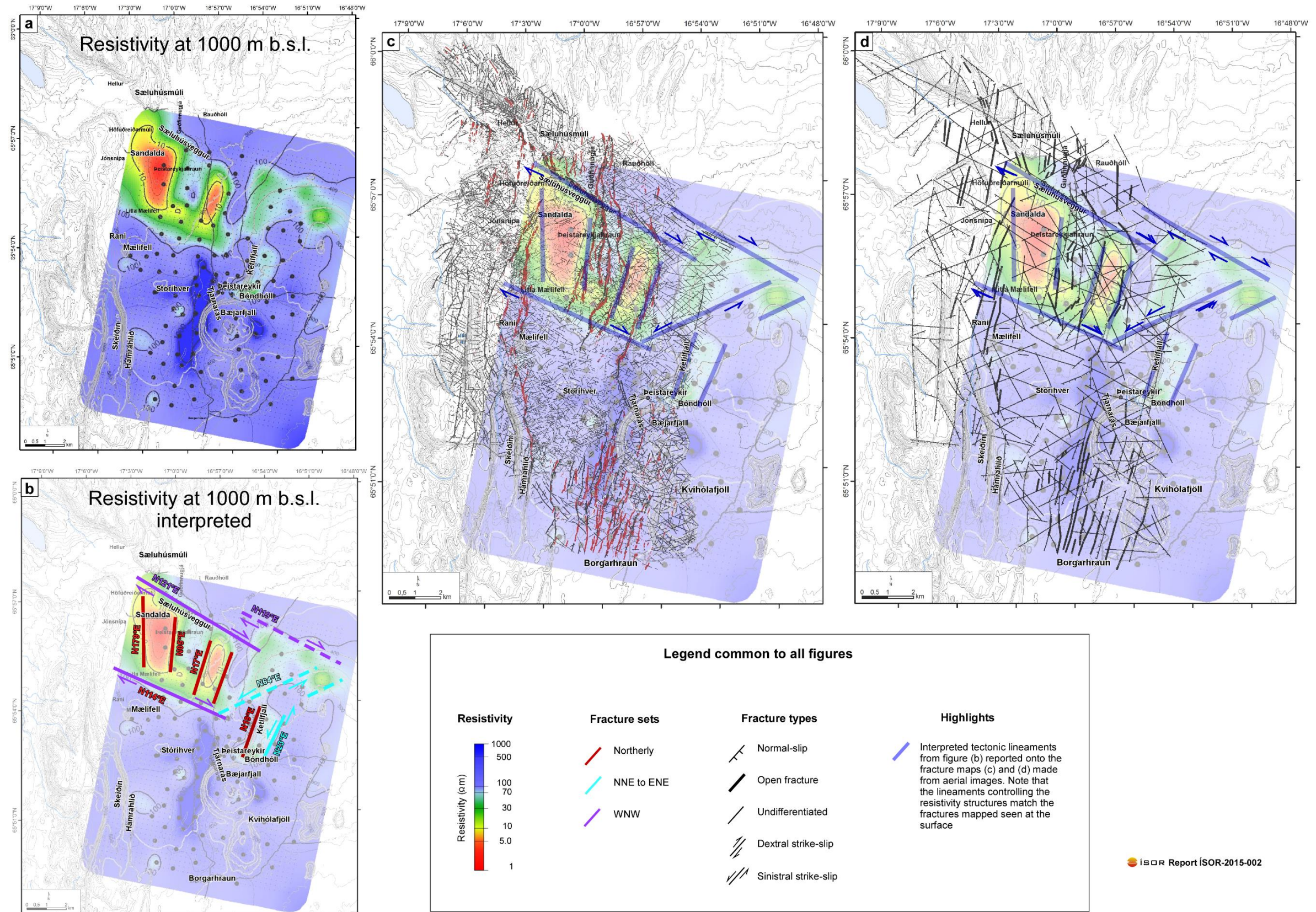


**Figure 15.** Structural interpretation of the resistivity structures at 1000 m b.s.l. (a) Un-interpreted resistivity map of Karlsdóttir et al. (2012) at 1000 m b.s.l. (b) Our structural interpretation of the resistivity structures. The interpreted lineaments from the resistivity structures superimposed on: (c) the fracture map, and (d) the interpreted weak zones by Khodayar and Björnsson (2013).

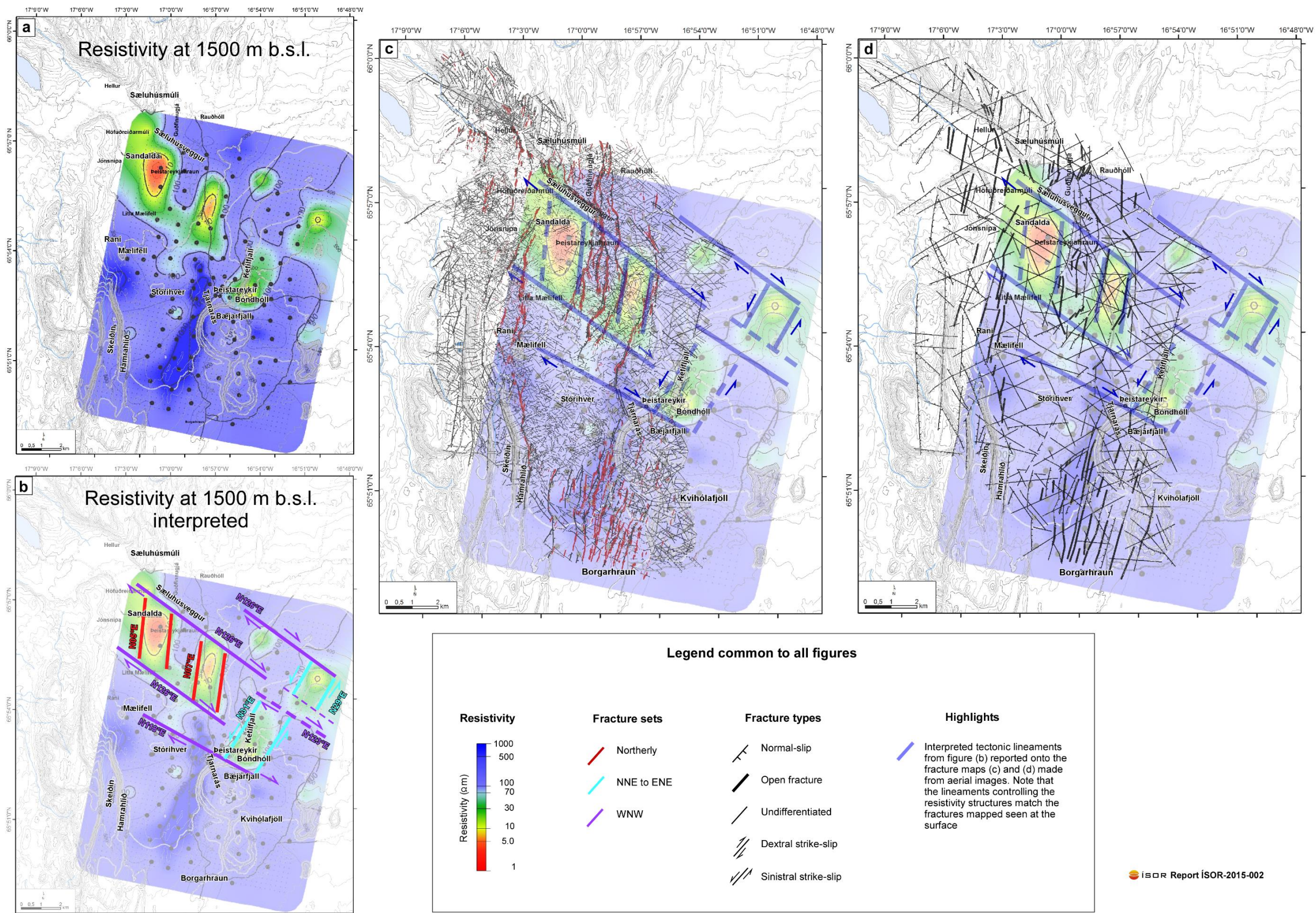


**Figure 16.** Structural interpretation of the resistivity structures at 1500 m b.s.l. (a) Un-interpreted resistivity map of Karlsdóttir et al. (2012) at 1500 m b.s.l. (b) Our structural interpretation of the resistivity structures. The interpreted lineaments from the resistivity structures superimposed on: (c) the fracture map, and (d) the interpreted weak zones by Khodayar and Björnsson (2013).

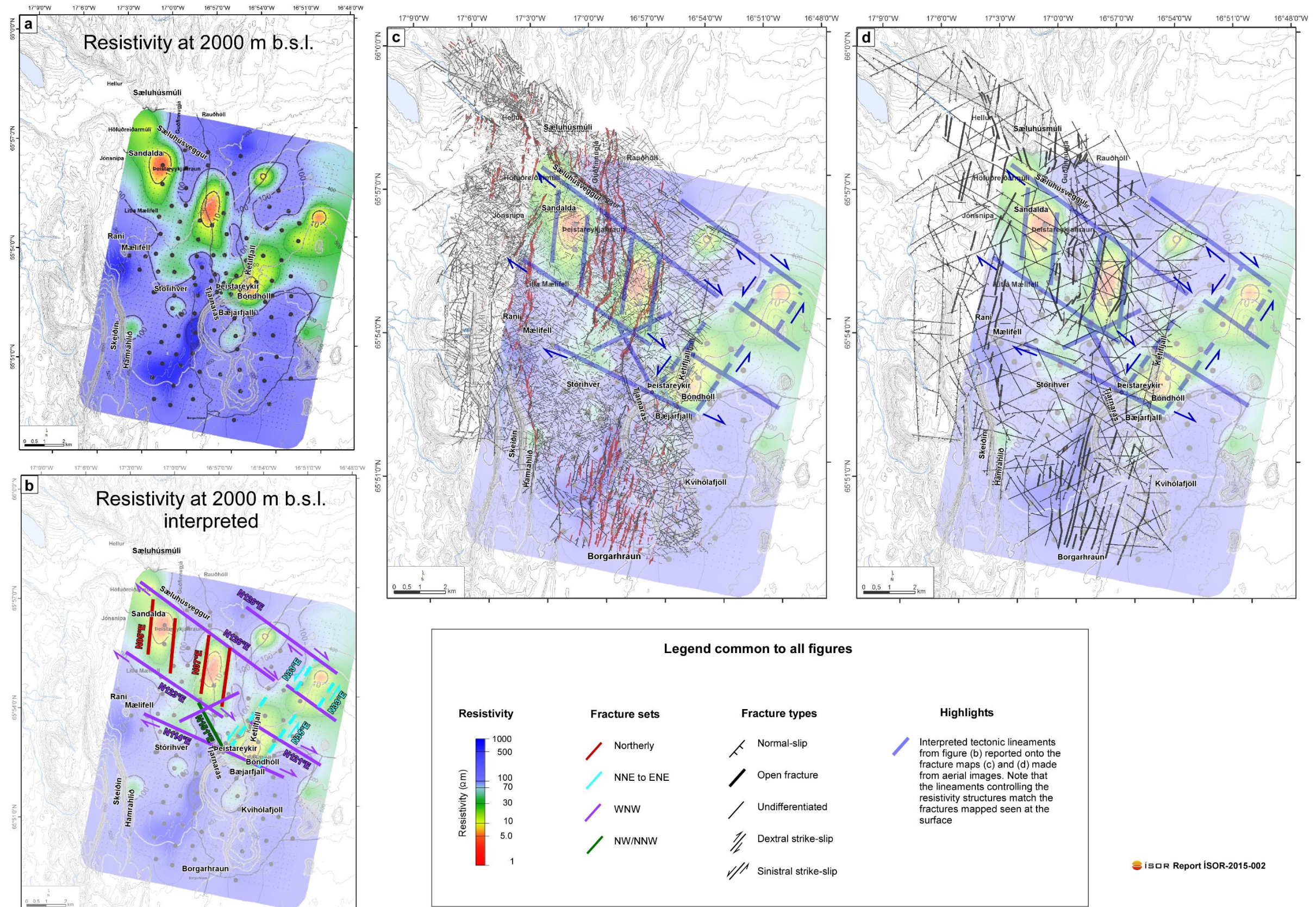


**Figure 17.** Structural interpretation of the resistivity structures at 2000 m b.s.l. (a) Un-interpreted resistivity map of Karlsdóttir et al. (2012) at 2000 m b.s.l. (b) Our structural interpretation of the resistivity structures. The interpreted lineaments from the resistivity structures superimposed on: (c) the fracture map, and (d) the interpreted weak zones by Khodayar and Björnsson (2013).

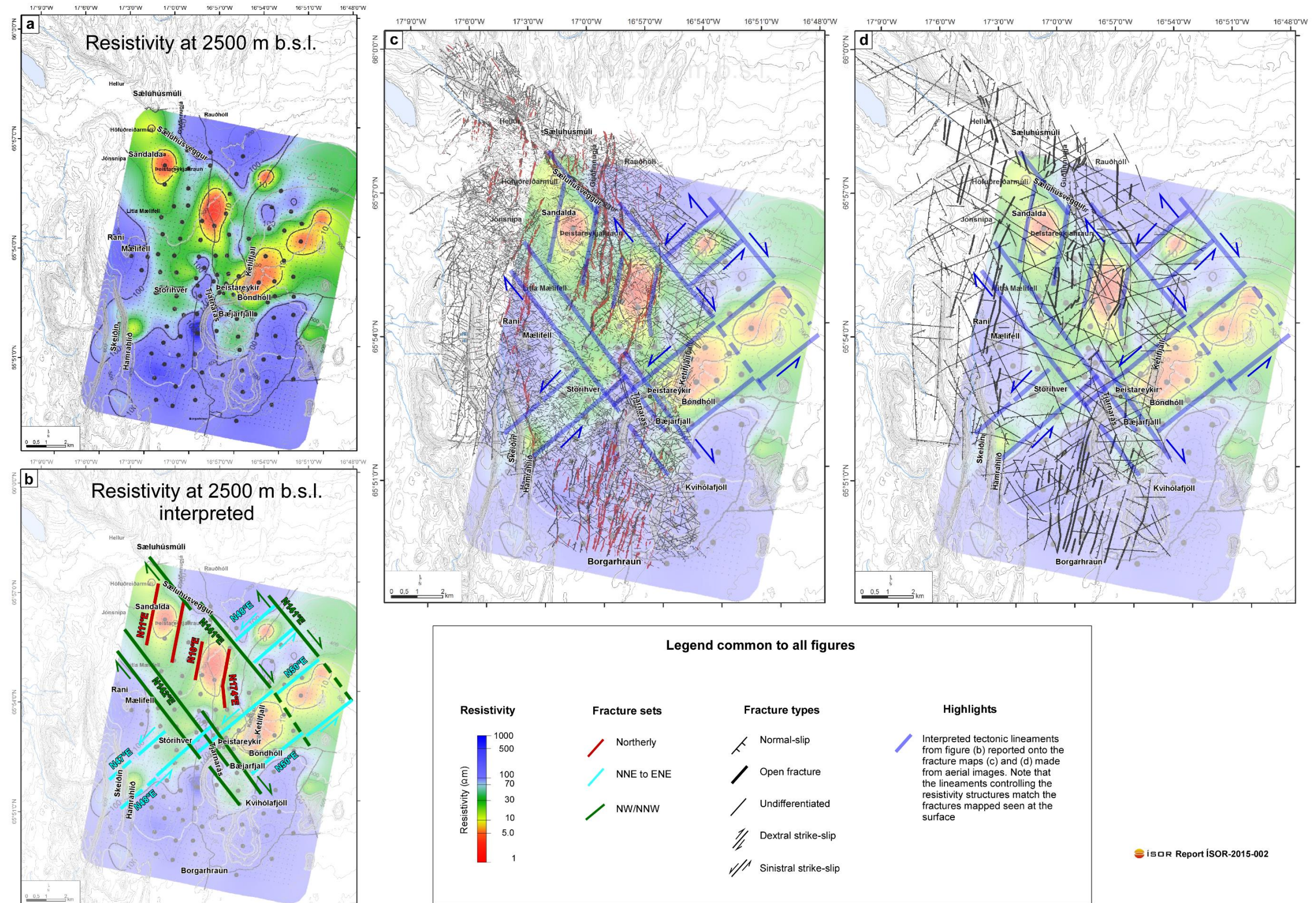


**Figure 18.** Structural interpretation of the resistivity structures at 2500 m b.s.l. (a) Un-interpreted resistivity map of Karlsdóttir et al. (2012) at 2500 m b.s.l. (b) Our structural interpretation of the resistivity structures. The interpreted lineaments from the resistivity structures superimposed on: (c) the fracture map, and (d) the interpreted weak zones by Khodayar and Björnsson (2013).

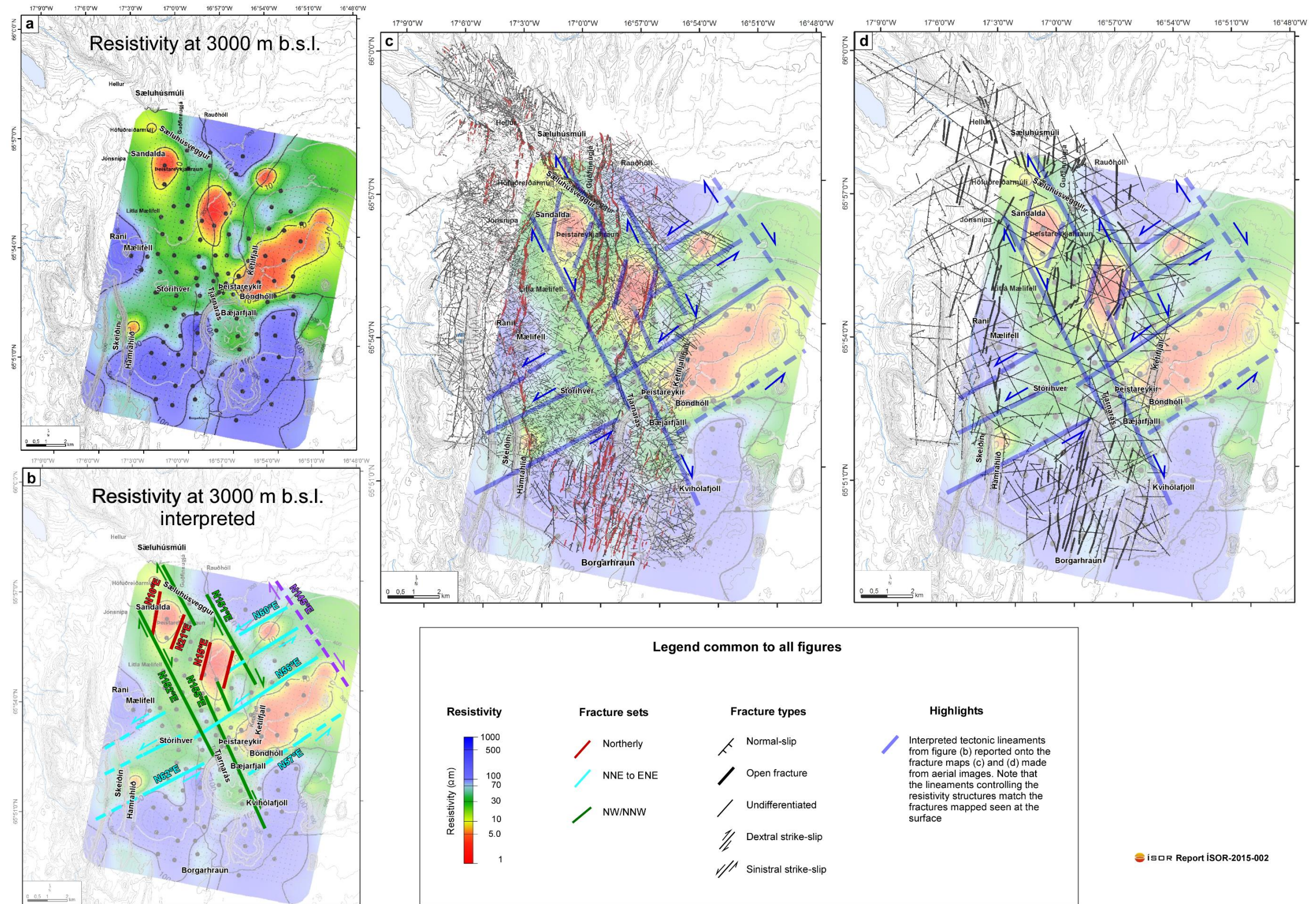


**Figure 19.** Structural interpretation of the resistivity structures at 3000 m b.s.l. (a) Un-interpreted resistivity map of Karlsdóttir et al. (2012) at 3000 m b.s.l. (b) Our structural interpretation of the resistivity structures. The interpreted lineaments from the resistivity structures superimposed on: (c) the fracture map, and (d) the interpreted weak zones by Khodayar and Björnsson (2013).

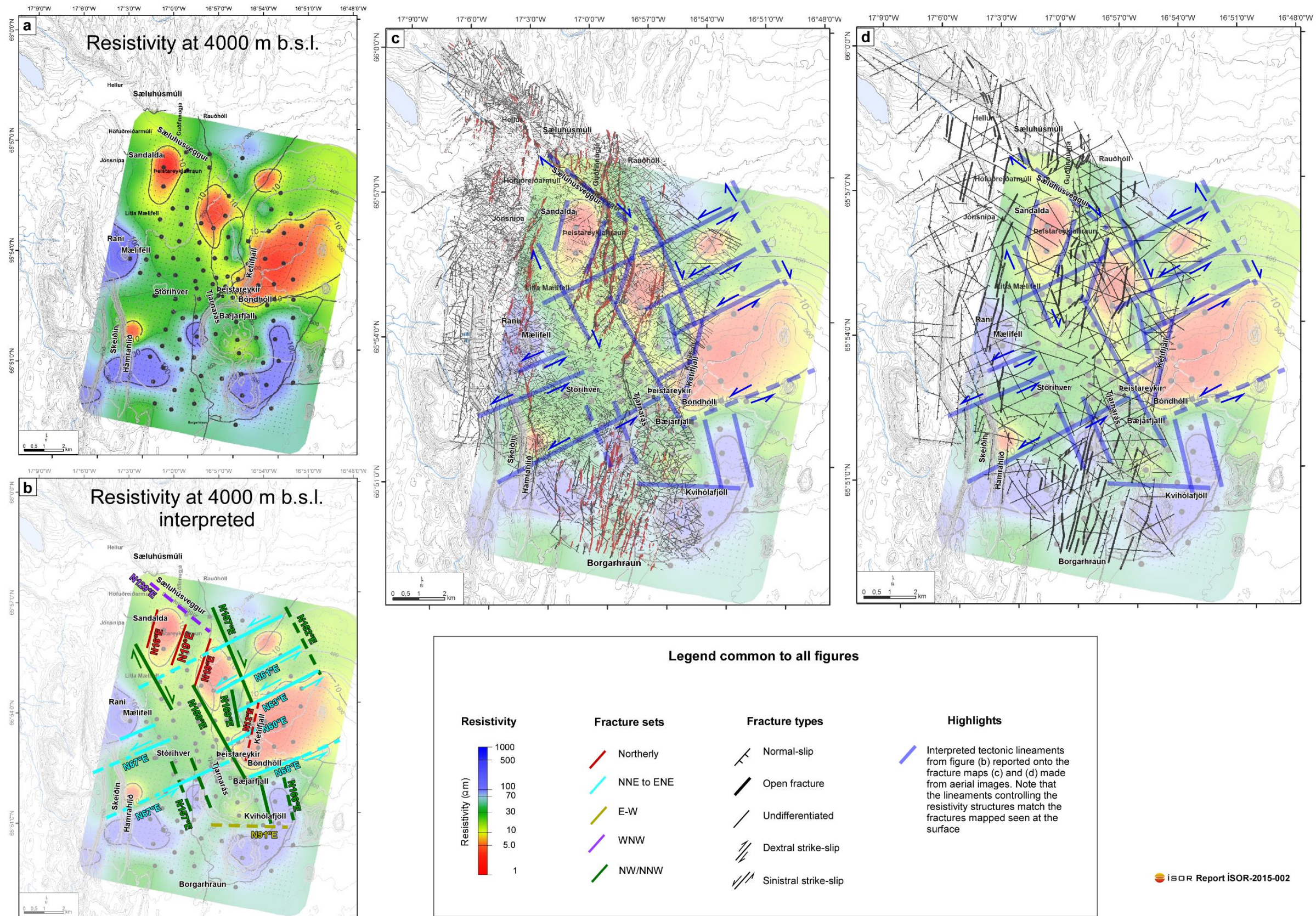


**Figure 20.** Structural interpretation of the resistivity structures at 4000 m b.s.l. (a) Un-interpreted resistivity map of Karlsdóttir et al. (2012) at 4000 m b.s.l. (b) Our structural interpretation of the resistivity structures. The interpreted lineaments from the resistivity structures superimposed on: (c) the fracture map, and (d) the interpreted weak zones by Khodayar and Björnsson (2013).

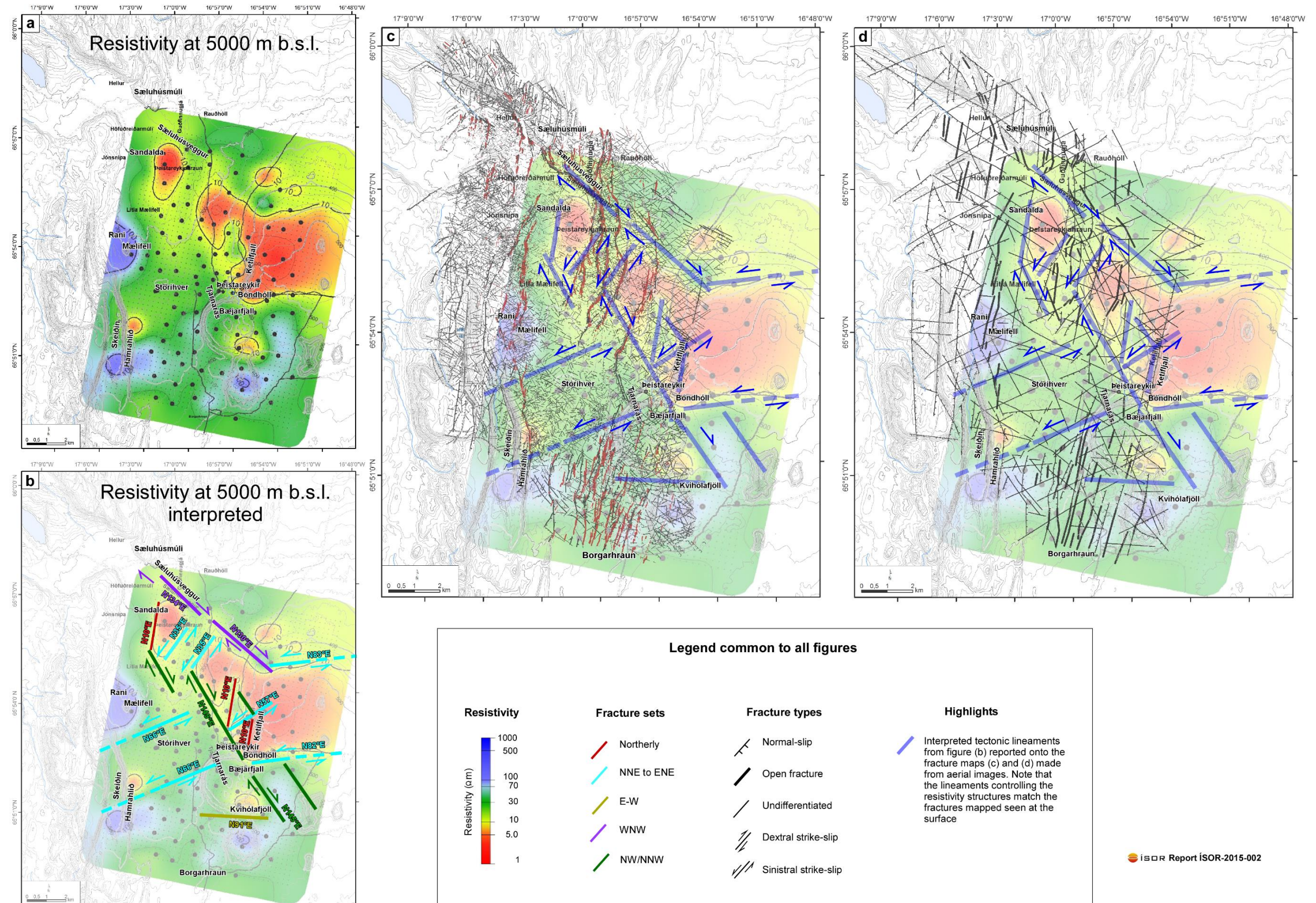


**Figure 21.** Structural interpretation of the resistivity structures at 5000 m b.s.l. (a) Un-interpreted resistivity map of Karlsdóttir et al. (2012) at 5000 m b.s.l. (b) Our structural interpretation of the resistivity structures. The interpreted lineaments from the resistivity structures superimposed on: (c) the fracture map, and (d) the interpreted weak zones by Khodayar and Björnsson (2013).



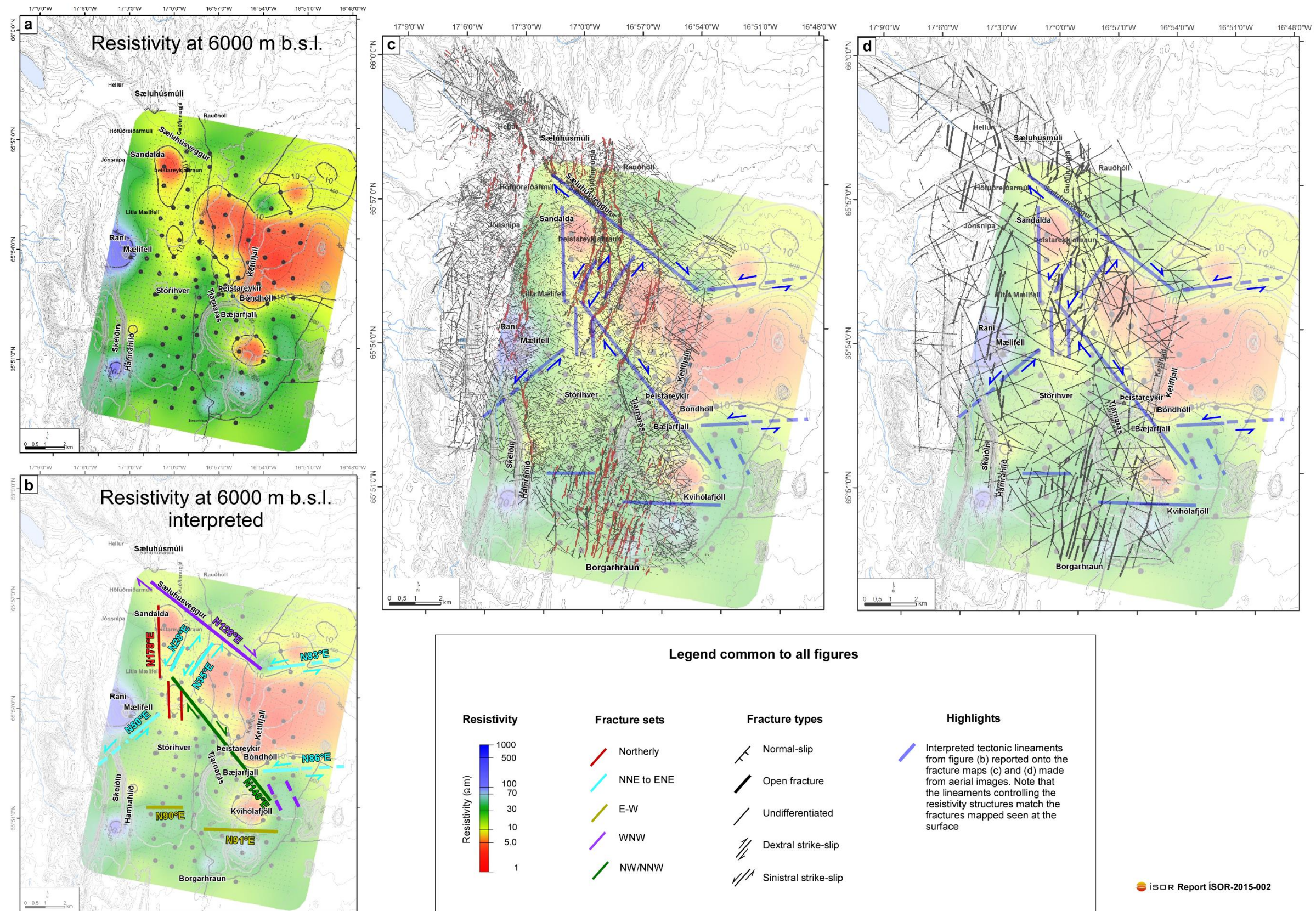


**Figure 22.** Structural interpretation of the resistivity structures at 6000 m b.s.l. (a) Un-interpreted resistivity map of Karlsdóttir et al. (2012) at 6000 m b.s.l. (b) Our structural interpretation of the resistivity structures. The interpreted lineaments from the resistivity structures superimposed on: (c) the fracture map, and (d) the interpreted weak zones by Khodayar and Björnsson (2013).

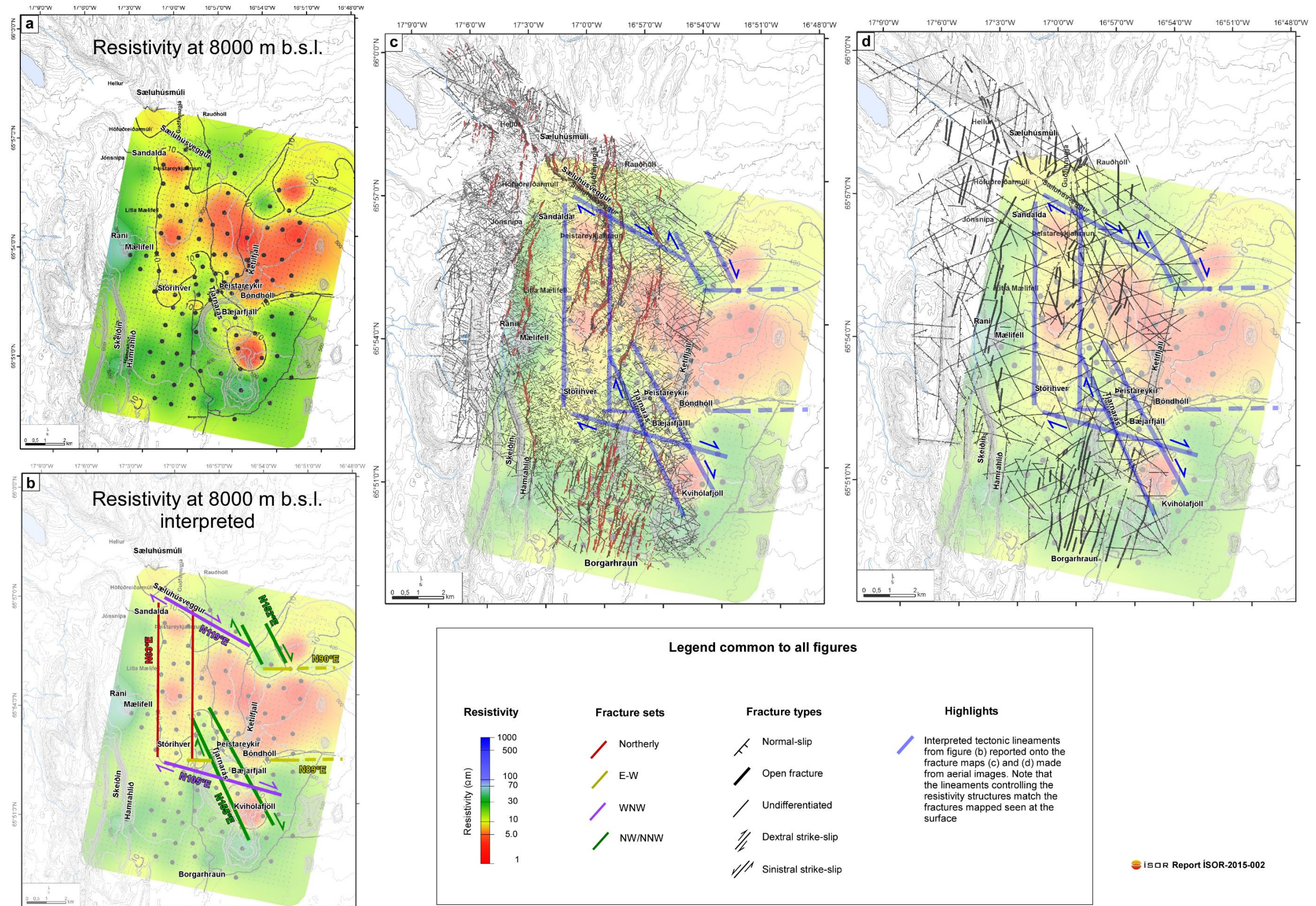


**Figure 23.** Structural interpretation of the resistivity structures at 8000 m b.s.l. (a) Un-interpreted resistivity map of Karlsdóttir et al. (2012) at 8000 m b.s.l. (b) Our structural interpretation of the resistivity structures. The interpreted lineaments from the resistivity structures superimposed on: (c) the fracture map, and (d) the interpreted weak zones by Khodayar and Björnsson (2013).

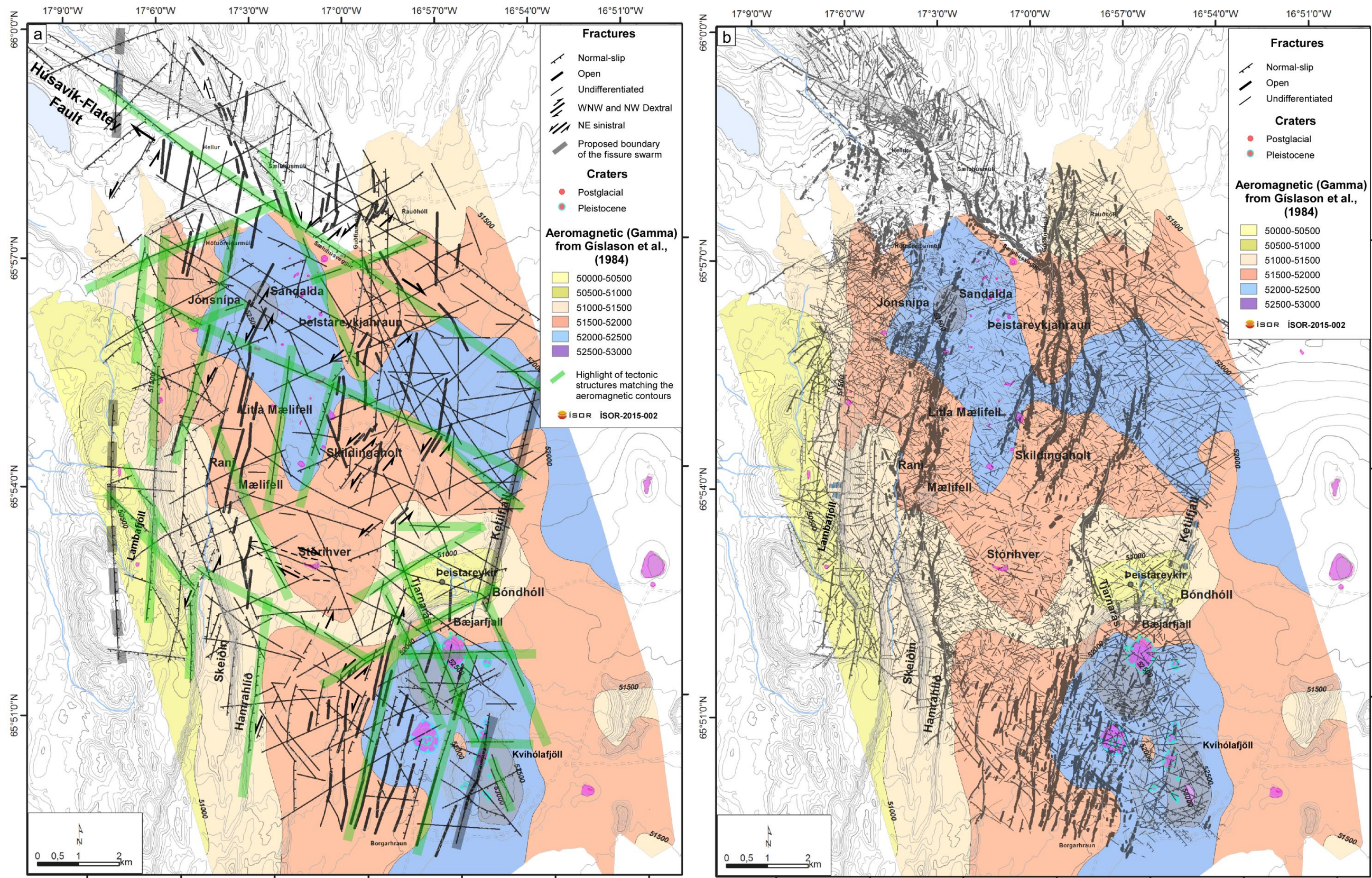


**Figure 24.** Structural interpretation of aeromagnetic data. Aeromagnetic background maps are from Gislason et al. (1984). (a) Interpreted structural weak zones from Khodayar and Björnsson (2013) superimposed on the aeromagnetic map with highlights of the structures that fit best the aeromagnetic contours. (b) Raw fracture map from Khodayar and Björnsson (2013) superimposed on the aeromagnetic map.

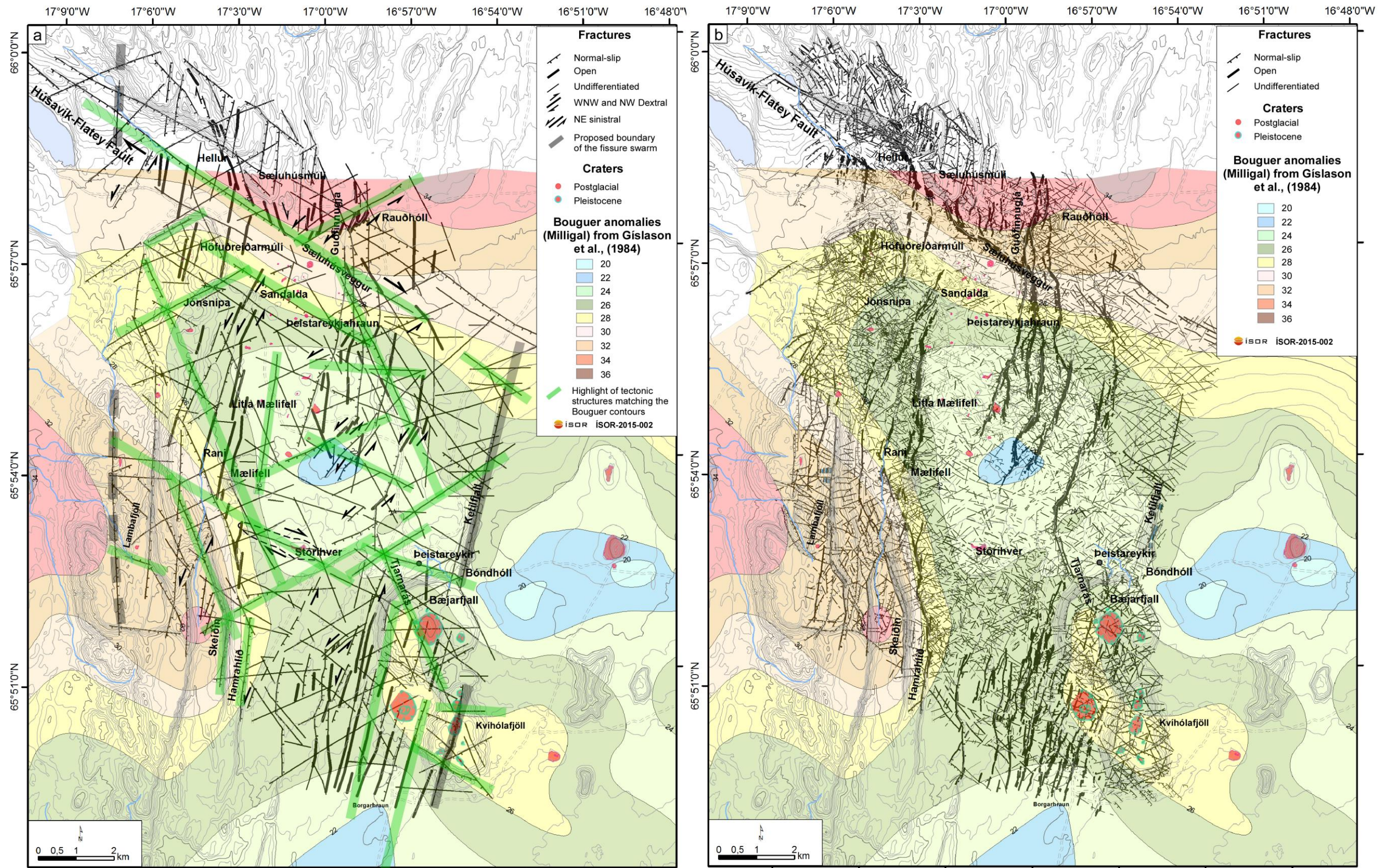


**Figure 25.** Structural interpretation of the Bouguer gravity map. The background Bouguer gravity maps are from Gíslason et al. (1984). (a) Interpreted structural weak zones from Khodayar and Björnsson (2013) superimposed on the Bouguer gravity map with highlights of the structures that fit best the Bouguer contours. (b) Raw fracture map from Khodayar and Björnsson (2013) superimposed on the Bouguer map.

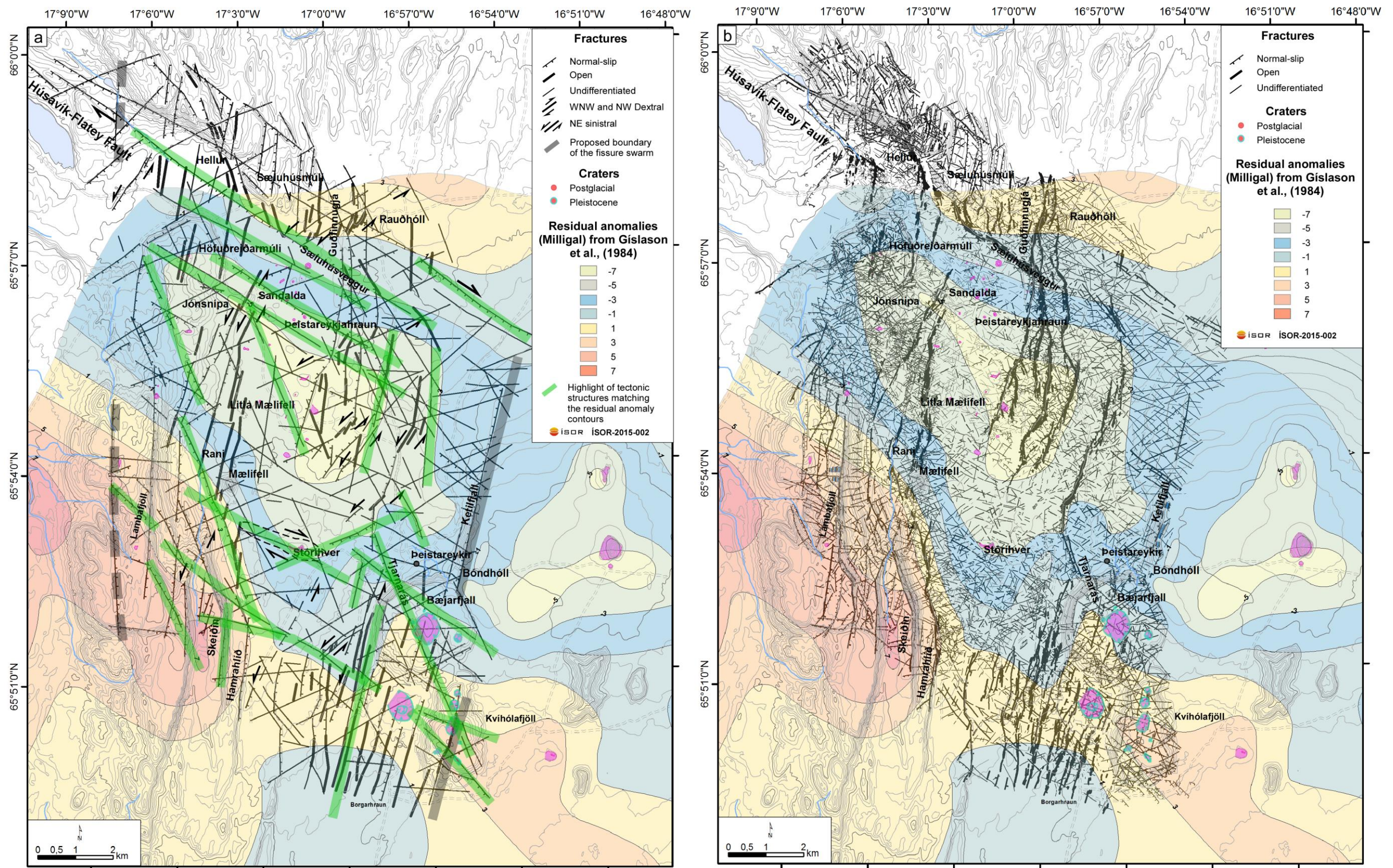


**Figure 26.** Structural interpretation of the Residual anomalies. The Residual anomaly background maps are from Gislason et al. (1984). (a) Interpreted structural weak zones from Khodayar and Björnsson (2013) superimposed on the Residual anomalies map with highlights of the structures that fit best the Residual contours. (b) Raw fracture map from Khodayar and Björnsson (2013) superimposed on the Residual map.